

A MODEL FOR INTERPRETATION OF BRINE-DEPENDENT SPONTANEOUS IMBIBITION EXPERIMENTS

S. EVJE^{A,*} AND A. HIORTH^B

ABSTRACT. Previous experimental results for spontaneous imbibition experiments in the context of chalk cores have revealed a rather puzzling behavior: The oil recovery curves, both the shape as well as the steady state level which is reached, depend strongly on the brine composition. In particular, it has been demonstrated that Mg^{2+} , SO_4^{2-} , and Ca^{2+} play a central role in this physico-chemical system. A good theoretical understanding of these experimental results, in terms of mathematical models that can suggest possible explanations of the lab experiments as well as predict behavior not yet tested in the lab, seems to still be lacking. The purpose of this paper is to try to shed light on some important modeling aspects. The model we propose is an extended version of the classical Buckley-Leverett (BL) equation for two-phase spontaneous imbibition where the water saturation equation has been coupled to a system of reaction-diffusion (RD) equations describing water-rock chemistry relevant for chalk core plugs. As far as water-rock chemistry is concerned we focus in this work on the combined effect of transport and dissolution/precipitation of calcite, magnesite, and anhydrite. The line we pursue is to couple changes of the wetting state, expressed in terms of the relative permeability and capillary pressure functions, to the water-rock chemistry behavior. More precisely, we build into the model the mechanism that the rock surface will become more water-wet at the places where dissolution of calcite takes place. In particular, we illustrate and analyze how different compositions of the imbibing brine then lead to different water-rock interaction scenarios which in turn gives qualitative and quantitative differences in the solution of the saturation equation describing spontaneous imbibition. Comparison with relevant experimental behavior is included as well as illustration of some possible interesting and non-trivial characteristic features of the model reflecting the nonlinear coupling mechanisms between the RD model for the water-rock chemistry and the BL equation for the water-oil transport.

Subject classification. 76T10, 76N10, 65M12, 35L65

Key words. water-rock chemistry, precipitation, dissolution, multiphase flow in porous media, wettability alteration, dynamic relative permeability, dynamic capillary pressure, non-equilibrium models, convection-diffusion-reaction equations

1. INTRODUCTION

Previous experimental studies of spontaneous imbibition for chalk core plugs have shown that seawater may change the wettability in the direction of more water-wet conditions in chalk reservoirs [37, 38, 41, 46, 3, 39, 47]. One possible explanation for this wettability alteration is that various ions (sulphate, calcium, magnesium, etc.) enter the formation water due to molecular diffusion. This creates a non-equilibrium state in the pore space that results in chemical reactions in the aqueous phase as well as possible water-rock interaction in terms of dissolution/precipitation of minerals and/or changes in surface charge. In turn, this paves the way for changes in the wetting state of the porous media in question.

Date: June 30, 2011.

^AUniversity of Stavanger, Prof. Olav Hanssensvei 15, NO-4068 Stavanger, Norway.

^BInternational Research Institute of Stavanger (IRIS), Prof. Olav Hanssensvei 15, NO-4068 Stavanger, Norway.

*Corresponding author.

Email address: steinar.evje@uis.no.

The authors acknowledge BP, ConocoPhillips, and the Ekofisk Coventurers, including TOTAL, ENI, Hydro, Statoil and Petoro, for supporting the work through the research center COREC. The research of the first author has also been supported by A/S Norske Shell.

In this work we will explore a mathematical model that allows for systematic studies of such *brine-dependent* spontaneous imbibition experiments. In particular, we shall employ the model and illustrate how it can be used to give a possible interpretation of some lab experiments reported in the work [47]. The purpose of that paper was to gain more understanding of the chemistry for improved spontaneous imbibition of different seawater like brines at low water wetness. It is believed that the water-rock chemistry can have a strong influence on the wetting state. For example, it has been proposed that the surface charge of chalk largely determines the wetting state. In other words, changing the brine composition can lead to a change of the surface charge, which in turn, can give a modified wetting state.

The main observation from the results shown in Fig. 1 is that the oil recovery level is highly sensitive to the brine composition, see also the figure text for more details. In particular, the characteristic role played by the different ions Mg^{2+} , SO_4^{2-} , and Ca^{2+} is clearly observed. More precisely, some main observations are:

- For brines with varying concentrations of sulphate ions SO_4^{2-} ranging from 0 to 4 times the seawater concentration, but without calcium Ca^{2+} and Mg^{2+} ions, the oil recovery is very low.
- Adding a seawater like concentration of Mg^{2+} to these brines give a strong increase in oil recovery. The increase in the oil recovery is strongly correlated to the concentration of SO_4^{2-} ions. Higher concentration of SO_4^{2-} leads to a more efficient imbibition process.
- Adding a seawater like concentration of Ca^{2+} to the brine Sw0x2S also gives an increase in oil recovery, although this increase is clearly much weaker compared to the cases where Mg^{2+} is added.

The core plugs were initially prepared such that they were preferentially oil-wet. At such wetting conditions no spontaneous imbibition of water will take place. Hence, the imbibition of water observed for certain brine compositions is attributed to a change of the wetting state towards more water-wet conditions.

More precisely, in the initial phase the cores are put under vacuum and saturated with fluid. The initial water is displaced by oil in a Hassler cell until a residual water saturation (Sw_r) of 20-35% is reached. The next step is ageing. The core is then left in a heated cabinet at 90°C for a period of 4-5 weeks to equilibrate the water with the oil and the rock. During this time the wettability of the core is changed from water wet to a mixed wettability state. After ageing, the core is placed in an imbibition cell. The aqueous phase that entirely surrounds the core is spontaneously imbibed into the core and oil is expelled. The chemistry of the imbibed water affects the amount of oil that is produced (expelled from the core). The production of oil in the spontaneous imbibition tests decreases to near zero after several weeks or months. When this occurs, the chemical parameters or the temperature of the system is usually changed. For example, the temperature is increased and/or the surrounding aqueous fluid is replaced with a fluid with a different chemical composition. When this is done the production of oil may increase. This is interpreted as a wettability change. The core is thought to have become more water-wet, and hence, more oil was expelled.

Modeling of two-phase spontaneous imbibition. Before we proceed it is instructive to mention some of the past and ongoing research activity relevant for spontaneous imbibition experiments. In [23] the authors derived approximate analytical solutions for the 1D model describing countercurrent imbibition of water and oil in different geometries and for water-wet media. Comparison with numerical approximations as well as experimental data was provided. A related work is represented by [13] where the authors study similarity solutions for the counter-current spontaneous imbibition two-phase model with a discontinuous permeability. In the work [34] wettability alteration was studied experimentally as a function of temperature. The experiments included spontaneous counter-current water imbibition as well as forced co-current water imbibition at various temperatures. Fines detachment was suggested as a mechanism for altering wettability. Another interesting work is represented by [42] where the authors study spontaneous imbibition and forced displacement for siliceous shale core plugs with different brines for naturally fractured low-permeability and intermediate to oil-wet surfaces. The main difference between the various

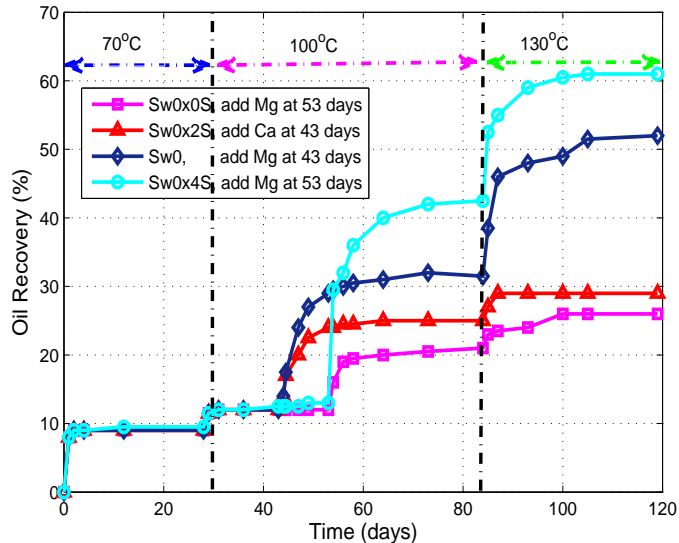


FIGURE 1. Oil recovery curves for imbibition tests on chalk cores where Mg^{2+} or Ca^{2+} (seawater concentrations) are added to the imbibing brine. Sw0 represents seawater without Mg^{2+} and Ca^{2+} whereas Sw0x0S is the same seawater but without SO_4^{2-} , Sw0x2S contains 2 times seawater concentration of SO_4^{2-} , and so on. Change of temperature is also involved. Plots have been reproduced from the work [47] by the accuracy of an eye and must be considered as approximate.

brines is the pH which is varied from 3 up to 12. It was observed that high and low pH gave a higher oil recovery than neutral pH. Simulations were performed indicating that the final recovery by spontaneous imbibition is determined by the characteristics of the capillary pressure as a function of water saturation.

One direction that has generated quite much interest more lately is the inclusion of so-called non-equilibrium effects in the relative permeability and capillary pressure functions. The concept of dynamic capillary pressure and relative permeability is introduced and has led to a rather intense experimental, modeling, and theoretical research, see [22] and references therein for a nice overview. Traditional formulations of multiphase flow rely on a straightforward extension of Darcy's equation for single-phase flow. The multiphase extension of Darcy's equation may be described as a quasi-linear relation, because the fluid flux depends linearly on the "driving force", which includes viscous, capillary, and gravity forces. All the nonlinearity is accounted for in the flow functions, that is, the relative permeability and capillary pressure functions [22]. In the mathematical formulation the saturation equation (for two-phase flow) is supplemented with an ode equation that accounts for the non-equilibrium effects.

In [35] the authors investigate inclusion of non-equilibrium effects in the estimation of relative permeability and capillary pressure from countercurrent imbibition experiments. It is concluded that non-equilibrium effects detected at laboratory scale influence the estimation of relative permeability and capillary pressure function. Similarly, in [27] a comparison is made between experimental data for spontaneous imbibition, respectively for counter-current and co-current flow, and simulations demonstrating that significant non-equilibrium effects are present. These works are in turn motivated by the seminal works [5, 36].

In our modeling approach we introduce a water-rock chemistry system, in terms of a transport-reaction model, that describes the evolution from a non-equilibrium state (which appears when the imbibing brine is mixed with the formation water) towards an equilibrium state where the flowing brine and rock inside the pore space is in chemical equilibrium. The behavior of this

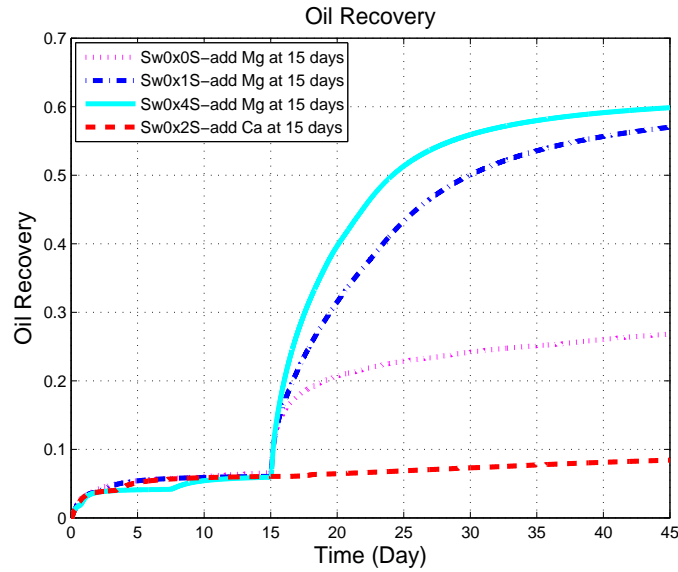


FIGURE 2. Oil recovery curves for imbibition tests on chalk cores performed at a constant temperature 130°C where Mg^{2+} or Ca^{2+} (seawater concentrations) are added to the imbibing brine after 15 days. Sw0 represents seawater without Mg^{2+} and Ca^{2+} whereas Sw0x0S is the same seawater but without SO_4^{2-} , Sw0x2S contains 2 times seawater concentration of SO_4^{2-} , and so on. The model simulations clearly reflect the special role played by magnesium ions Mg^{2+} as a wettability modifying ion in the presence of sulphate ions SO_4^{2-} .

system is coupled to the wetting state of the rock represented by the relative permeability and capillary pressure functions. In this particular sense the proposed model involves dynamic relative permeability and capillary pressure functions.

Previous modeling of wettability alteration. As an attempt to increase the understanding of experimental results dealing with wettability alteration in chalk reservoirs, see [37, 38, 41, 46, 3, 39, 47] and references therein, some modeling work has been carried out more recently. A 1D mathematical model for simulation of dynamic wettability alteration in spontaneous imbibition experiments has been established [44, 45]. The model represents a core plug on laboratory scale where a general wettability alteration (WA) agent is added. The term WA agent is used to represent a single ion or group of ions. Thus, we truncate all the complicated chemical interactions into a single adsorption function. Relative permeability and capillary pressure curves are constructed by employing an interpolation between two sets of generic curves corresponding to oil-wet and water-wet conditions. However, this model does not include any link to a more detailed water-rock chemistry model. Consequently, such models do not seem capable to explain the experimental results shown in Fig. 1 where different brines give very different oil recovery curves. Similar type of models have been proposed and studied in [43] and [21], respectively, in the study of viscous fingering phenomena on reservoir scale and low salinity water flooding behavior. A main feature of the current model (and contrary to the works [21, 43, 44, 45]) is that the imbibition process is sensitive to the chemical composition of the invading brine. In other words, a doubling of the sulphate concentration will have a direct impact on the dissolution/precipitation processes, which in turn affects the imbibition process and corresponding oil recovery.

Objective. The objective of this paper is to demonstrate one possible interpretation of the spontaneous imbibition experiments as reported in [47] and shown in Fig. 1 by employing a model based on the one that was first developed in [15]. Main building blocks in the model are:

- Combining (i) a reaction-diffusion model that describes water-rock chemistry relevant for chalk core plugs; (ii) the classical Buckley-Leverett model used to describe spontaneous imbibition;
- Alterations in the wetting state is taken into account by linking changes in the flow functions (relative permeability and capillary pressure functions) to changes in the mineral composition inside the core. This is motivated by calculations from the work [20]. As a consequence the wettability alteration is controlled by the water-rock chemistry;
- The resulting model allows for systematic studies of the role played by the important ions Ca^{2+} , Mg^{2+} , and SO_4^{2-} on the behavior of the spontaneous imbibition experiments.

In Fig. 2 we show the oil recovery curves obtained by applying the model that will be described in the next section. One difference between the simulated results and the experimental data is that the temperature is kept constant at 130° C. This is done in order to avoid varying too many parameters in the mathematical model. Most importantly, we observe that the model is able to capture some of the main trends in terms of oil recovery as a function of brine composition, see the text below Fig 2. In the numerical section we shall give a more detailed description of the water saturation behavior corresponding to the oil recovery curves appearing in Fig. 2. The role played by the brine composition as a controlling mechanism for the wettability alteration will then be demonstrated.

2. THE WATER-ROCK CHEMISTRY MODEL

Let Ω be the domain of the core composed of calcite CaCO_3 and define the molar concentrations of the different species in the units of mol/liter:

$$\begin{array}{llll}
 \rho_c = [\text{CaCO}_3] \text{ (solid)} & C_{ca} = [\text{Ca}^{2+}] \text{ (ions)} & C_h = [\text{H}^+] & \text{(ions)} \\
 \rho_g = [\text{CaSO}_4] \text{ (solid)} & C_{mg} = [\text{Mg}^{2+}] \text{ (ions)} & C_{oh} = [\text{OH}^-] & \text{(ions)} \\
 \rho_m = [\text{MgCO}_3] \text{ (solid)} & C_{so} = [\text{SO}_4^{2-}] \text{ (ions)} & C_{hco} = [\text{HCO}_3^-] & \text{(ions)} \\
 & C_{na} = [\text{Na}^+] \text{ (ions)} & C_{co} = [\text{CO}_3^{2-}] & \text{(ions)} \\
 & C_{cl} = [\text{Cl}^-] \text{ (ions)} & &
 \end{array}$$

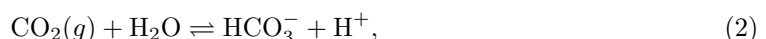
The primary unknowns are the concentration of minerals represented by ρ (mol per liter rock): ρ_c , ρ_g , ρ_m ; and concentration of species represented by C (mol per liter of solution): C_{ca} , C_{so} , C_{mg} , C_{na} , C_{cl} , C_h , C_{oh} , C_{co} , and C_{hco} . Hence, the concentration C of a species expressed in terms of mol per liter rock is given by $\phi s C$ where ϕ is porosity and s is water saturation. We shall assume that the Na^+ and Cl^- ions do not take part in the chemical reactions, i.e., their concentrations C_{na} and C_{cl} are determined by the transport mechanisms only (molecular diffusion). We include chemical kinetics associated with the concentrations ρ_c , ρ_g , ρ_m , C_{ca} , C_{so} , C_{mg} involved in the water-rock interactions (dissolution/precipitation), whereas the concentrations C_h , C_{oh} , C_{co} , and C_{hco} involved in the aqueous chemistry, are obtained by considering equilibrium state equations.

2.1. Preliminaries. In the following, we first give some more details concerning the equilibrium chemistry associated with the chemical reactions (2)–(4), the aqueous chemistry. Then we describe the relations that take into account kinetics associated with the precipitation/dissolution processes (15)–(17). In particular, we shall distinguish between concentration C and chemical activity a noting that they are related by [26, 1]

$$a = \gamma C, \tag{1}$$

where γ is the activity coefficient. We refer to Appendix A for further details how to calculate the γ 's for different brines.

2.2. Aqueous chemistry (chemical reactions in the liquid phase). The following chemical reactions relevant for the aqueous chemistry are included:



We do not include reaction kinetic associated with these chemical reactions but assume that they are at equilibrium. In other words, it is implicitly assumed that they take place at a much faster time scale than the dissolution/precipitation processes (15)–(17). We will show below how we use the equilibrium equations for these chemical reactions to determine the concentrations of HCO_3^- , H^+ , CO_3^{2-} and OH^- which are species in the water phase:

First, it is assumed in the water-rock chemistry model that we know the concentrations C_{na} and C_{cl} since these are not reactive. In particular, we also assume that the CO_2 partial pressure P_{CO_2} is known, from which the CO_2 concentration can be determined. More precisely, the local equilibrium associated with (2) gives the relation

$$C_1 = P_{\text{CO}_2} K = a_{hco} a_h = (\gamma_{hco} \gamma_h) C_{hco} C_h, \quad (5)$$

for an appropriate choice of the equilibrium constant K and P_{CO_2} . The chemical reaction equation (3) gives us

$$C_2 = \frac{a_{co} a_h}{a_{hco}} = \left(\frac{\gamma_{co} \gamma_h}{\gamma_{hco}} \right) \frac{C_{co} C_h}{C_{hco}}, \quad (6)$$

where C_2 is a known equilibrium constant. Moreover, the reaction equation (4) gives

$$C_w = a_h a_{oh} = (\gamma_{oh} \gamma_h) C_{oh} C_h, \quad (7)$$

where C_w is known. The following aqueous charge balance equation should hold for the various species contained in the water

$$\sum_i C_i Z_i = 0, \quad (8)$$

where Z_i refers to the ionic charge of species i . For the system in question, this results in the following balance equation:

$$2C_{ca} + 2C_{mg} + C_h + C_{na} = 2C_{so} + C_{hco} + 2C_{co} + C_{oh} + C_{cl}. \quad (9)$$

Thus, the four equations (5)–(8) allow us to solve for C_h , C_{hco} , C_{co} , and C_{oh} . This relation can be written in the form

$$C_3 = C_{hco} + 2C_{co} + C_{oh} - C_h, \quad (10)$$

where

$$C_3 = C_3(C_{ca}, C_{mg}, C_{so}; C_{na}, C_{cl}) = 2(C_{ca} + C_{mg} - C_{so}) + (C_{na} - C_{cl}). \quad (11)$$

It's convenient to introduce the following notation:

$$\tilde{C}_1 = \frac{C_1}{\gamma_{hco} \gamma_h}, \quad \tilde{C}_2 = \frac{C_2 \gamma_{hco}}{\gamma_{co} \gamma_h}, \quad \tilde{C}_w = \frac{C_w}{\gamma_h \gamma_{oh}}. \quad (12)$$

We shall make use of the simplifying assumption that the concentration C_{co} of CO_3^{2-} is relatively low and can be neglected in the charge balance equation (10). Clearly, (10) can then be written in the form

$$C_3 = C_{hco} + \frac{\tilde{C}_w}{C_h} - C_h, \quad (13)$$

where we have used (7). Combining (5) and (13) we get

$$C_3 = \frac{\tilde{C}_1 + \tilde{C}_w}{C_h} - C_h,$$

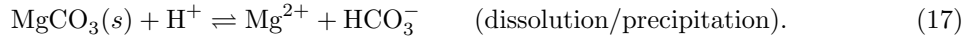
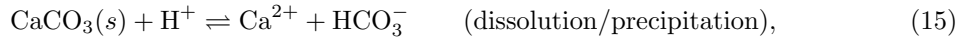
which results in the second order equation $C_h^2 + C_3 C_h - (\tilde{C}_1 + \tilde{C}_w) = 0$. The relevant solution is then given by

$$C_h = \frac{1}{2} \left(-C_3 + \sqrt{C_3^2 + 4(\tilde{C}_1 + \tilde{C}_w)} \right), \quad C_{hco} = \frac{\tilde{C}_1}{C_h}. \quad (14)$$

Finally, C_{co} and C_{oh} can be determined from the equations (6) and (7). In particular, we note that $C_h = C_h(C_{ca}, C_{so}, C_{mg}; C_{na}, C_{cl})$, in view of (11).

Remark 1. Concerning the above consideration that the CO_2 partial pressure P_{CO_2} is known, we should add that, generally speaking, this is a somewhat strong assumption that need to be addressed in more detail. However, it turns out that for the cases we have investigated calcite dissolution is coupled mainly to magnesite formations. When calcium and carbonate are released from the rock, magnesium combines with carbonate to form magnesite, and there seems to be a small net change in the CO_2 concentration in this process. Formation of anhydrite could lead to some net change in the CO_2 concentration, but for the cases we have looked at, the dominant effect seems to be calcite dissolution due to magnesite precipitation. There could also be some partitioning of CO_2 between the water and oil phase. However, we would like to address these issues in more detail in forthcoming works.

2.3. Water-rock interaction (dissolution and precipitation). The water-rock chemistry system represents a reactive transport system with three mineral phases ($CaCO_3$, $CaSO_4$, $MgCO_3$) and three aqueous species (Ca^{2+} , SO_4^{2-} , Mg^{2+}) which react according to basic kinetic laws. More precisely, the chemical reactions we include are:



We shall include reaction kinetic (rate equations) relevant for these processes which allows us to study non-equilibrium behavior associated with our water-rock chemistry system. The rate equations associated with the water-rock interaction, as described by the dissolution/precipitation processes (15)–(17), are obtained by following an approach similar to that in [7, 14], see also references therein like [26] (chapter 1) and [40, 31]. The main point of this approach is the use of an empirical rate equation of the form

$$R = k(1 - \Omega), \quad (18)$$

where R is the rate, k is an empirical fitting term, and $(1 - \Omega)$ the degree of disequilibrium with the mineral in question. Ω is the ratio of the ion activity product (IAP) to the solubility product K for the solid in question, that is, $\Omega = \text{IAP}/K$. If $0 < 1 - \Omega$ the solution is undersaturated which may lead to dissolution; if $0 > 1 - \Omega$ the solution is supersaturated which implies precipitation.

Thus, the reaction terms \dot{r}_i , for $i = c, g, m$ associated with (15)–(17), are given as follows where we have used $n = 1$ in (18):

$$\dot{r}_c = k_1^c a_c - k_{-1}^c \frac{a_{ca} a_{hco}}{a_h} = k_1^c \left(1 - \frac{a_{hco} a_{ca}}{K^c a_h}\right) = k_1^c \left(1 - \left[\frac{\gamma_{ca} C_1}{\gamma_h^2 K^c}\right] \frac{C_{ca}}{C_h^2}\right), \quad (19)$$

$$\dot{r}_g = k_1^g a_g - k_{-1}^g a_{ca} a_{so} = k_1^g \left(1 - \frac{a_{ca} a_{so}}{K^g}\right) = k_1^g \left(1 - \left[\frac{\gamma_{ca} \gamma_{so}}{K^g}\right] C_{ca} C_{so}\right), \quad (20)$$

$$\dot{r}_m = k_1^m a_m - k_{-1}^m \frac{a_{mg} a_{hco}}{a_h} = k_1^m \left(1 - \left[\frac{\gamma_{mg} C_1}{\gamma_h^2 K^m}\right] \frac{C_{mg}}{C_h^2}\right), \quad (21)$$

where

$$K^c = \frac{k_1^c}{k_{-1}^c}, \quad K^g = \frac{k_1^g}{k_{-1}^g}, \quad K^m = \frac{k_1^m}{k_{-1}^m}. \quad (22)$$

Here a_j represents chemical activity associated with species j . Moreover, we have supposed that the minerals exist as pure phases which implies that the ion activities of the minerals are one, see for example [7]. That is, we have set $a_c = a_g = a_m = 1$ in (19)–(21). k_{-1}^j represents the rate of precipitation whereas k_1^j represents the rate of dissolution associated with the different species $j = c, g, m$ corresponding to $CaCO_3$, $CaSO_4$, and $MgCO_3$. Similarly, K^j is used to represent the equilibrium constant associated with $j = c, g, m$. These are known values. On the other hand, much less is known about the rate of precipitation/dissolution represented by k_{-1}^j and k_1^j . It is

convenient to introduce the notation (where we have skipped the dependency on C_{cl} and C_{na})

$$\begin{aligned} F_c(C_{ca}, C_{so}, C_{mg}) & \stackrel{\text{def}}{=} \left(1 - \left[\frac{\gamma_{ca} C_1}{\gamma_h^2 K^c}\right] \frac{C_{ca}}{C_h^2}\right), \\ F_g(C_{ca}, C_{so}) & \stackrel{\text{def}}{=} \left(1 - \left[\frac{\gamma_{ca} \gamma_{so}}{K^g}\right] C_{ca} C_{so}\right), \\ F_m(C_{ca}, C_{so}, C_{mg}) & \stackrel{\text{def}}{=} \left(1 - \left[\frac{\gamma_{mg} C_1}{\gamma_h^2 K^m}\right] \frac{C_{mg}}{C_h^2}\right). \end{aligned} \quad (23)$$

Then we get the following rate equations associated with the minerals represented by ρ_c , ρ_g , and ρ_m (mole per liter rock):

$$\begin{aligned} \frac{d\rho_c}{dt} & = -\dot{r}_c = -k_1^c F_c(C_{ca}, C_{so}, C_{mg}), \\ \frac{d\rho_g}{dt} & = -\dot{r}_g = -k_1^g F_g(C_{ca}, C_{so}, C_{mg}), \\ \frac{d\rho_m}{dt} & = -\dot{r}_m = -k_1^m F_m(C_{ca}, C_{so}, C_{mg}). \end{aligned} \quad (24)$$

Similarly, (19)–(21) give rise to the following set of rate equations associated with the aqueous species C_{ca} , C_{so} , and C_{mg} involved in the precipitation/dissolution processes (15)–(17) and expressed in terms of mole per liter rock consistent with (24):

$$\begin{aligned} \frac{d(\phi s C_{ca})}{dt} & = \dot{r}_{ca} = \dot{r}_c + \dot{r}_g = k_1^c F_c(C_{ca}, C_{so}, C_{mg}) + k_1^g F_g(C_{ca}, C_{so}, C_{mg}), \\ \frac{d(\phi s C_{so})}{dt} & = \dot{r}_{so} = \dot{r}_g = k_1^g F_g(C_{ca}, C_{so}, C_{mg}), \\ \frac{d(\phi s C_{mg})}{dt} & = \dot{r}_{mg} = \dot{r}_m = k_1^m F_m(C_{ca}, C_{so}, C_{mg}). \end{aligned} \quad (25)$$

An important modification is to take into account the fact that mineral dissolution stops once the mineral has disappeared [7, 14]. To build this mechanism into the rate equations given by (19)–(21), we use (23) and change these equations in the following manner:

$$\begin{aligned} \dot{r}_c & = k_1^c \left[\text{sgn}^+(\rho_c) F_c^+(C_{ca}, C_{so}, C_{mg}) - F_c^-(C_{ca}, C_{so}, C_{mg}) \right], \\ \dot{r}_g & = k_1^g \left[\text{sgn}^+(\rho_g) F_g^+(C_{ca}, C_{so}, C_{mg}) - F_g^-(C_{ca}, C_{so}, C_{mg}) \right], \\ \dot{r}_m & = k_1^m \left[\text{sgn}^+(\rho_m) F_m^+(C_{ca}, C_{so}, C_{mg}) - F_m^-(C_{ca}, C_{so}, C_{mg}) \right], \end{aligned} \quad (26)$$

where

$$\begin{aligned} \text{sgn}^+(x) & = \begin{cases} 1, & \text{if } x \geq 0; \\ 0, & \text{otherwise,} \end{cases} \\ F_I & = F_I^+ - F_I^-, \quad \text{where } F_I^+ = \max(0, F_I), \quad F_I^- = \max(0, -F_I). \end{aligned}$$

Clearly, in view of (24), we see that for $F_I < 0$ where $I = c, g, m$ represents the mineral in question, the mineral precipitates; for $F_I = 0$ chemical equilibrium exists and nothing happens; for $F_I > 0$ the mineral dissolves, but only as long as the mineral exists, i.e., $\rho_I > 0$.

3. COUPLING OF WETTABILITY ALTERATION TO CHEMICAL CHANGES ON THE ROCK SURFACE

The idea behind the proposed model is to build into the model a mechanism that allows chemical based changes on the rock surface to induce changes in the wetting state from an preferentially oil-wet to a more water-wet surface. For that purpose we must specify relative permeability and capillary pressure functions that can represent, respectively, the oil-wet and water-wet surface. This approach has been employed in works like [44, 45, 43, 21]. The following description is similar to the presentation of the model given in [15], however, for completeness of this work we have included it.

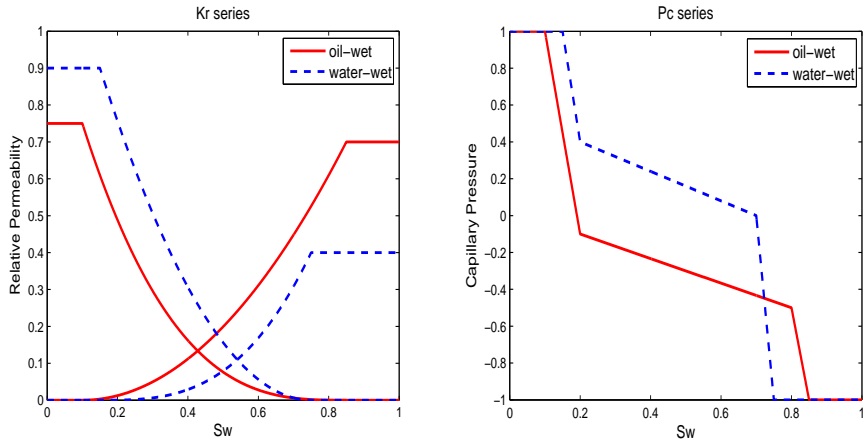


FIGURE 3. **Left:** Relative permeability curves corresponding to preferentially oil-wet and water-wet conditions. **Right:** Capillary pressure curves corresponding to oil-wet (mixed-wet) and water-wet like conditions.

3.1. Relative permeability and capillary pressure functions. As a basic model the well-known Corey type correlations are used [11]. They are given in the form (dimensionless functions)

$$\begin{aligned} k(s) &= k^* \left(\frac{s - s_{wr}}{1 - s_{or} - s_{wr}} \right)^{Nk}, & s_{wr} \leq s \leq 1 - s_{or}, \\ k_o(s) &= k_o^* \left(\frac{1 - s_{or} - s}{1 - s_{or} - s_{wr}} \right)^{Nk_o}, & s_{wr} \leq s \leq 1 - s_{or}, \end{aligned} \quad (27)$$

where s_{wr} and s_{or} represent critical saturation values and Nk and Nk_o are the Corey exponents that must be specified. In addition, k^* and k_o^* are the end point relative permeability values that also must be given.

As a simple model for capillary pressure a piecewise linear function of the following form is used

$$P_c(s) = P^* \begin{cases} 1 & s < s_{wr}, \\ 1 + \left(\frac{pc_1 - 1}{s_1 - s_{wr}} \right) (s - s_{wr}) & s_{wr} \leq s \leq s_1, \\ pc_1 + \left(\frac{pc_2 - pc_1}{s_2 - s_1} \right) (s - s_1) & s_1 \leq s \leq s_2, \\ pc_2 + \left(\frac{-1 - pc_2}{1 - s_{or} - s_2} \right) (s - s_2) & s_2 \leq s \leq 1 - s_{or}, \\ -1 & s > 1 - s_{or}, \end{cases} \quad (28)$$

where P^* and the points (s_1, pc_1) and (s_2, pc_2) are constants that must be specified. In a more realistic setting these would be based on experimental data and, typically, more than two points would be given. Furthermore, P^* is a scaling constant (characteristic capillary pressure) that contains information about interfacial tension and contact angle effects. More precisely, $P_c(s) = P^* J(s)$, where the dimensionless function $J(s)$ is called the Leverett function and its multiplier P^* takes the form [11, 36, 27]

$$P^* = \frac{\sigma \cos(\theta)}{\sqrt{\kappa/\phi}}, \quad (29)$$

where σ is interfacial tension, θ is contact angle, κ absolute permeability, ϕ porosity. In Appendix B the data required to obtain concrete relative permeability and capillary pressure curves are specified that can represent, respectively, preferentially oil-wet and water-wet conditions. We refer to Fig. 3 for an illustration of these saturation dependent flow functions.

3.2. Dissolution of calcite as a mechanism for wettability alteration. In the paper [20] the effect of pore water chemistry on surface charge and wettability was discussed. A surface complexation model was presented in order to predict the surface charge and potential of calcite

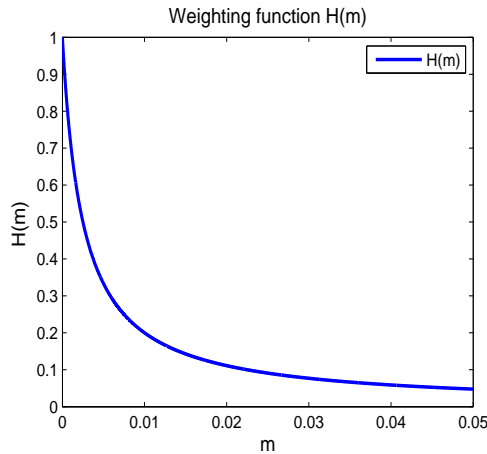


FIGURE 4. The weighting function $H(m)$ as defined by (31) with $r = 400$. The choice of r determines how much calcite that must be dissolved to bring forth a certain change of the wetting state.

exposed to different brines. One of the key results in that paper was the observation that surface charge of calcite had the wrong temperature dependence in order to explain the release of oil from the calcite surface. In particular the calcite surface charge was positive and increasing when it was exposed to formation water and seawater at temperatures in the range of 25C to 130°C. Thus the attraction between the negative oil phase and positive calcite surface charge would increase as temperature increased. However in the experimental data the opposite trend was observed; release of oil and enhanced imbibition of water was observed as temperature was systematically increased. Based on this observation, in [20] it was then suggested that dissolution of calcite could explain the enhanced imbibition of water and expulsion of oil. If dissolution takes place exactly where the oil is attached, one could imagine that a fresh water wet calcite surface is exposed after dissolution has taken place. A linear correlation was found between the amounts of expelled oil and expected (calculated) dissolution of calcite. The dissolution was a consequence of precipitation of secondary minerals. Thus at the current stage the model does not distinguish between wettability change due to dissolution of the primary mineral calcite or the formation of the secondary minerals magnesite and anhydrite. In order to distinguish between those two mechanisms, experiments should be performed where calcite is dissolved without any formation of secondary minerals.

We now describe how we link dissolution of calcite to change of the wetting state. Having an initial concentration ρ_0 of a mineral with concentration ρ , we define the quantity $m(\rho)$

$$m(\rho) := \max(\rho_0 - \rho, 0) \quad (30)$$

as a measure for the dissolved mineral. In the following, motivated by the work [20] as explained above, we associated ρ with calcite. Moreover, we define

$$H(\rho) := \frac{1}{1 + rm(\rho)}, \quad (31)$$

where $r > 0$ is a specified constant. In view of (30) it follows that the function $H(\rho)$ becomes a weighting function such that

- (i) $0 < H(\rho) \leq 1$, for $\rho \geq 0$;
- (ii) $H(\rho) = 1$, for $\rho \geq \rho_0$ (precipitation);
- (iii) $0 < H(\rho) < 1$ for $\rho < \rho_0$ (dissolution).

How fast $H(\rho)$ is approaching 0 as $m(\rho)$ is increasing, depends on the choice of r . In the numerical investigations in Section 5 we use $r = 400$. See Fig. 4 for a plot of this function. Now, the weighting

function $H(\rho)$ can be used to represent the wetting state in the core plug; $H(\rho) = 1$ corresponds to the initial preferentially oil-wet state, whereas $H(\rho) \approx 0$ represents the water-wet state.

Improved oil recovery by invasion of seawater in a preferential oil-wet porous medium is ultimately due to changes in various flow parameters. The flow conditions before and after the wettability alteration can be described by capillary pressure curves, relative permeability curves, and residual saturations. Wettability alteration is incorporated in these flow parameters by defining capillary pressure $P_c(s, \rho_c)$ and relative permeability curves $k(s, \rho_c), k_o(s, \rho_c)$ through an interpolation between the oil-wet and water-wet curves specified in Appendix B and shown in Fig. 3.

More precisely, motivated by the proposed hypothesis that transition from preferentially oil-wet towards water-wet conditions depends on where dissolution of calcite (CaCO_3) takes place, the following interpolation is proposed:

$$k(s, \rho_c) = H(\rho_c)k^{ow}(s) + [1 - H(\rho_c)]k^{ww}(s), \quad (32)$$

where $H(\rho_c)$ is defined by (31) and ρ_c is the calcite concentration. Hence, when no dissolution of CaCO_3 has taken place it follows that $H(\rho_c) = 1$, implying that $k(s, \rho_c) = k^{ow}(s)$. This reflects the initial preferential oil-wet wetting state. Then, as dissolution of CaCO_3 takes place, it follows that $m(\rho_c)$ increases. In particular, if the dissolution effect $m(\rho_c)$ becomes large enough $H(\rho_c) \approx 0$, which means that $k(s, \rho_c) \approx k^{ww}(s)$, reflecting that a wettability alteration has taken place which results in a water-wet wetting state. The same interpolation procedure is natural to use for the capillary pressure curve. That is,

$$P_c(s, \rho_c) = H(\rho_c)P_c^{ow}(s) + [1 - H(\rho_c)]P_c^{ww}(s). \quad (33)$$

Thus, different concentrations of ρ_c below its initial concentration $\rho_{c,0}$ as measured by $m(\rho_c)$, produce capillary pressure curves that lie between the two extremes $P_c^{ow}(s)$ and $P_c^{ww}(s)$.

4. THE COUPLED TWO-PHASE FLOW AND WATER-ROCK CHEMISTRY MODEL

Mass conservation considerations for the water-oil system with water-rock chemistry gives rise to the following transport-reaction system [15]

$$\begin{aligned} \partial_t(\phi s_o C_o) + \nabla \cdot (C_o \mathbf{V}_o) &= 0, \\ \partial_t(\phi s C_l) + \nabla \cdot (C_l \mathbf{V}_l) &= 0, \\ \partial_t(\phi s C_{na}) + \nabla \cdot (C_{na} \mathbf{V}_g) &= 0, \\ \partial_t(\phi s C_{cl}) + \nabla \cdot (C_{cl} \mathbf{V}_g) &= 0, \\ \partial_t(\phi s C_{ca}) + \nabla \cdot (C_{ca} \mathbf{V}_g) &= \dot{r}_c + \dot{r}_g, \\ \partial_t(\phi s C_{so}) + \nabla \cdot (C_{so} \mathbf{V}_g) &= \dot{r}_g, \\ \partial_t(\phi s C_{mg}) + \nabla \cdot (C_{mg} \mathbf{V}_g) &= \dot{r}_m, \\ \partial_t \rho_c &= -\dot{r}_c, \\ \partial_t \rho_g &= -\dot{r}_g, \\ \partial_t \rho_m &= -\dot{r}_m, \end{aligned} \quad (34)$$

where C_l and C_o are concentrations of water and oil, respectively, with respect to the volume of the pore space occupied by water and oil. \mathbf{V}_o , \mathbf{V}_l and \mathbf{V}_g represent, respectively, fluid velocity associated with oil, water, and ions. Following along the line of [15, 44, 14], see also references therein, we employ Darcy's law and Fick's law and reformulate the model (34) such that it takes

the following form:

$$\begin{aligned}
\partial_t(\phi s_o C_o) + \nabla \cdot (C_o \mathbf{V}_o) &= 0, \\
\partial_t(\phi s C) + \nabla \cdot (C \mathbf{V}) &= (\dot{r}_c + 2\dot{r}_g + \dot{r}_m), \\
\partial_t(\phi s C_{na}) + \nabla \cdot (C_{na} \mathbf{V}) &= \nabla \cdot (D \nabla C_{na}), \\
\partial_t(\phi s C_{cl}) + \nabla \cdot (C_{cl} \mathbf{V}) &= \nabla \cdot (D \nabla C_{cl}), \\
\partial_t(\phi s C_{ca}) + \nabla \cdot (C_{ca} \mathbf{V}) &= \nabla \cdot (D \nabla C_{ca}) + (\dot{r}_c + \dot{r}_g), \\
\partial_t(\phi s C_{so}) + \nabla \cdot (C_{so} \mathbf{V}) &= \nabla \cdot (D \nabla C_{so}) + \dot{r}_g, \\
\partial_t(\phi s C_{mg}) + \nabla \cdot (C_{mg} \mathbf{V}) &= \nabla \cdot (D \nabla C_{mg}) + \dot{r}_m, \\
\partial_t \rho_c &= -\dot{r}_c, \\
\partial_t \rho_g &= -\dot{r}_g, \\
\partial_t \rho_m &= -\dot{r}_m,
\end{aligned} \tag{35}$$

$$\mathbf{V} = -\kappa \lambda (\nabla p - \rho g \nabla d), \quad \mathbf{V}_o = -\kappa \lambda_o (\nabla p_o - \rho_o g \nabla d), \quad \lambda = \frac{k}{\mu}, \quad \lambda_o = \frac{k_o}{\mu_o}.$$

Here $C = C_l + C_{na} + C_{cl} + C_{ca} + C_{so} + C_{mg}$ represents the brine concentration, κ is the absolute permeability, λ, λ_o fluid mobilities, k, k_o are relative permeability functions, p pressure, μ, μ_o fluid viscosities, ρ, ρ_o fluid densities, g gravity constant, and d is the vertical distance for a reference level to the point (x, y, z) . Moreover, $D = D(\phi, s)$ is the diffusion coefficient (based on Archie's law) given by

$$D = D(\phi, s) = D_m \phi^p s^q I, \quad 1 \leq p, q \leq 2.5. \tag{36}$$

The coefficient p is referred to as the cementation exponent, q as the saturation exponent. The cementation exponent is often close to 2 whereas the saturation exponent is also often fixed at a value in the same range, see for example [9, 12, 6].

Relying on a fractional flow formulation a 1D model that includes viscous forces, capillary forces, and gravity has been derived in [15] based on (35), and we refer to that work for details. Main assumptions that are used are:

- The oil and water component densities C_o and C are assumed to be constant, i.e., incompressible fluids;
- The effect from the chemical reactions in the water phase equation (second equation of (35)) is neglected which is reasonable since the concentration of the water phase C is much larger than the concentrations of the ion exchange involved in the chemical reactions;
- Constant porosity ϕ , absolute permeability κ , viscosities μ, μ_o ;
- One dimensional flow in a vertical domain is assumed. Note, however, that for the numerical calculations in Section 5 we ignore gravity since main focus is on spontaneous imbibition where capillarity is the driving force. Investigations of gravity effects are left to another work.

Then, we obtain a two-phase model with inclusion of water-rock chemistry of the form

$$\begin{aligned}
\partial_t(\phi s) + \partial_x F(s, \rho_c) &= \partial_x (A(s, \rho_c) \partial_x P_c(s, \rho_c)), \\
\partial_t(\phi s C_{na}) + \partial_x (C_{na} F(s, \rho_c)) &= \partial_x (D \partial_x C_{na}) + \partial_x (C_{na} A(s, \rho_c) \partial_x P_c(s, \rho_c)), \\
\partial_t(\phi s C_{cl}) + \partial_x (C_{cl} F(s, \rho_c)) &= \partial_x (D \partial_x C_{cl}) + \partial_x (C_{cl} A(s, \rho_c) \partial_x P_c(s, \rho_c)), \\
\partial_t(\phi s C_{ca}) + \partial_x (C_{ca} F(s, \rho_c)) &= \partial_x (D \partial_x C_{ca}) + \partial_x (C_{ca} A(s, \rho_c) \partial_x P_c(s, \rho_c)) + (\dot{r}_c + \dot{r}_g), \\
\partial_t(\phi s C_{so}) + \partial_x (C_{so} F(s, \rho_c)) &= \partial_x (D \partial_x C_{so}) + \partial_x (C_{so} A(s, \rho_c) \partial_x P_c(s, \rho_c)) + \dot{r}_g, \\
\partial_t(\phi s C_{mg}) + \partial_x (C_{mg} F(s, \rho_c)) &= \partial_x (D \partial_x C_{mg}) + \partial_x (C_{mg} A(s, \rho_c) \partial_x P_c(s, \rho_c)) + \dot{r}_m, \\
\partial_t \rho_c &= -\dot{r}_c, \\
\partial_t \rho_g &= -\dot{r}_g, \\
\partial_t \rho_m &= -\dot{r}_m,
\end{aligned} \tag{37}$$

where

$$\begin{aligned} F(s, \rho_c) &= v_T f(s, \rho_c) + g \Delta \rho \kappa G(s, \rho_c), & G(s, \rho_c) &= [f \lambda_o](s, \rho_c) \\ A(s, \rho_c) &= -\kappa G(s, \rho_c). \end{aligned} \quad (38)$$

Here $v_T = v_T(t)$ is the sum of the water and oil velocity V and V_o and must be constant in space. $f = \lambda/(\lambda + \lambda_o)$ is the standard water fractional flow function, $\Delta \rho = \rho - \rho_o$ the difference in fluid densities, $P_c = p_o - p$ is the capillary pressure function. Note that the relative permeability functions $k(s, \rho_c)$, $k_o(s, \rho_c)$ and capillary pressure $P_c(s, \rho_c)$ introduce a dependence on the concentration of calcite ρ_c , as explained in Section 3, in addition to the dependence on the water saturation s . Consequently, the water-oil transport mechanism described by the first equation of (37) is coupled to the water-rock chemistry system described by second to eight equations of (37).

Counter-current flow. In the following we shall assume that the two-phase flow takes place as *counter-current flow*, i.e., the total velocity v_T is zero inside the core, $v_T = 0$. This assumption is reasonable in light of the fact that the experiments we want to simulate involve spontaneous imbibition in a 1D domain where the two open faces of the core are in contact with the brine and the main driving force is capillary diffusion. Implicitly, it is assumed that when water imbibes the advancing water displaces from the pore space an equal volume of oil, which flows back to the surface of the core and escapes through the inlet. Thus, capillarity causes equal and opposite flows of the fluids, and this process is referred to as counter-current imbibition. We refer to the works [23, 33, 36, 27, 35] (and references therein) for interesting discussions related to modeling of counter-current flow.

Scaled version of the model. Let τ (s) be the time scale of the problem. Then, an appropriate space scale could be given by the diffusive typical length L (m)

$$L = \sqrt{\overline{D}_m \tau}, \quad (39)$$

where \overline{D}_m (m²/s) is a reference diffusion coefficient. We then define dimensionless space x' and time t' variables as follows

$$x' = \frac{x}{\sqrt{\overline{D}_m \tau}}, \quad t' = \frac{t}{\tau}. \quad (40)$$

We introduce reference viscosity $\overline{\mu}$ (Pa s) and capillary pressure $\overline{P}_c = P^*$ (Pa). Then we define dimensionless coefficients

$$D'_m = \frac{D_m}{\overline{D}_m}, \quad \mu' = \frac{\mu}{\overline{\mu}}, \quad \mu'_o = \frac{\mu_o}{\overline{\mu}}, \quad P'_c = \frac{P_c}{\overline{P}_c} = J, \quad \lambda'_o = \frac{k_o}{\mu'_o}. \quad (41)$$

Rewriting (37) in terms of the dimensionless space and time variables (40) and using (41), the following form of the system is obtained (skipping the prime notation)

$$\partial_t(\phi s) + \gamma \partial_x F(s, u) = \varepsilon \partial_x (A(s, u) \partial_x J(s, u)), \quad (42)$$

$$\begin{aligned} \partial_t(\phi s C_{na}) + \gamma \partial_x (C_{na} F(s, \rho_c)) &= \delta \partial_x (\phi^p s^q \partial_x C_{na}) + \varepsilon \partial_x (C_{na} A(s, \rho_c) \partial_x J(s, \rho_c)), \\ \partial_t(\phi s C_{cl}) + \gamma \partial_x (C_{cl} F(s, \rho_c)) &= \delta \partial_x (\phi^p s^q \partial_x C_{cl}) + \varepsilon \partial_x (C_{cl} A(s, \rho_c) \partial_x J(s, \rho_c)), \end{aligned} \quad (43)$$

$$\partial_t(\phi s C_{ca}) + \gamma \partial_x (C_{ca} F(s, \rho_c)) = \delta \partial_x (\phi^p s^q \partial_x C_{ca}) + \varepsilon \partial_x (C_{ca} A(s, \rho_c) \partial_x J(s, \rho_c)) + \tau(\dot{r}_c + \dot{r}_g),$$

$$\partial_t(\phi s C_{so}) + \gamma \partial_x (C_{so} F(s, \rho_c)) = \delta \partial_x (\phi^p s^q \partial_x C_{so}) + \varepsilon \partial_x (C_{so} A(s, \rho_c) \partial_x J(s, \rho_c)) + \tau \dot{r}_g,$$

$$\partial_t(\phi s C_{mg}) + \gamma \partial_x (C_{mg} F(s, \rho_c)) = \delta \partial_x (\phi^p s^q \partial_x C_{mg}) + \varepsilon \partial_x (C_{mg} A(s, \rho_c) \partial_x J(s, \rho_c)) + \tau \dot{r}_m,$$

$$\partial_t \rho_c = -\tau \dot{r}_c,$$

$$\partial_t \rho_g = -\tau \dot{r}_g, \quad (44)$$

$$\partial_t \rho_m = -\tau \dot{r}_m,$$

with

$$F(s, \rho_c) = [f \lambda_o](s, \rho_c), \quad A(s, \rho_c) = -[f \lambda_o](s, \rho_c), \quad (45)$$

and where the dimensionless characteristic numbers γ and ε , sometimes referred to as, respectively, the *gravity number* and the *capillary number*, are given by

$$\gamma = \frac{L\Delta\rho\kappa g}{\bar{\mu}D_m}, \quad \varepsilon = \frac{\kappa\bar{P}_c}{\bar{\mu}D_m}, \quad \delta = D_m. \quad (46)$$

We choose $\bar{D}_m = D_m$ in (41) such that $D'_m = 1$ and $\delta = 1$.

Boundary and initial conditions. In order to have a well defined system to solve we must specify appropriate initial and boundary conditions. Both faces of the core are exposed to a brine with specified concentrations of the various species, hence, it is natural to use the Dirichlet condition

$$s(0^-, t) = s(1^+, t) = 1.0, \quad C_i(0^-, t) = C_i(1^+, t) = C_i^*, \quad (47)$$

for the species $i = na, cl, ca, so, mg$ where C_i^* is the specified ion concentrations of the brine that is used. For countercurrent flow it seems to be a well accepted choice that we have zero-capillary pressure [33] because of the continuity of the capillary pressure at the imbibition face. In other words, we have the boundary condition

$$J(t)|_{x=0^-} = J(t)|_{x=1^+} = 0. \quad (48)$$

Concerning the five equations (43) for the concentrations C_i , it is assumed that molecular diffusion is the only force that makes the species enter at the open faces of the plug. In other words, we use the condition that

$$\gamma[C_i F(s, \rho_c)] - \varepsilon[C_i A(s, \rho_c)\partial_x J(s, \rho_c)] = 0, \quad \text{for } x = 0, 1. \quad (49)$$

Initially, the plug is filled with oil and a certain amount of formation water. Thus, initial data are given by

$$s|_{t=0}(x) = s_{\text{init}}(x), \quad x \in [0, 1],$$

and for the ions $i = na, cl, ca, so, mg$,

$$\begin{aligned} C_i|_{t=0}(x) &= C_{i0}, \\ \rho_c|_{t=0}(x) &= \rho_{c0}, \quad \rho_g|_{t=0}(x) = \rho_{g0}, \quad \rho_m|_{t=0}(x) = \rho_{m0}, \quad x \in [0, 1], \end{aligned} \quad (50)$$

for given initial concentration of the species C_{i0} in the water phase and prescribed initial mineral concentrations ρ_{c0} , ρ_{g0} , and ρ_{m0} .

Numerical discretization. The numerical scheme that is employed for solving the system (42)–(44) together with the initial and boundary data (47)–(50), is based on a splitting approach where we alternate between solving (i) a convection-diffusion system accounting for the transport effects; (ii) solving an ODE system accounting for the chemical reactions (dissolution/precipitation). The details are given in [15], see also [44, 14]. We also refer to [28] for more information of operator splitting as a numerical method for transport-reaction models.

5. NUMERICAL INVESTIGATIONS

The objective of the numerical computations is to demonstrate how the proposed coupling between the water-rock chemical system and the two-phase flow functions (relative permeability and capillary pressure) gives an extended version of the Buckley-Leverett model that predicts *brine-dependent* spontaneous imbibition results. In particular, we are interested in the role played by Ca^{2+} , Mg^{2+} , and SO_4^{2-} ion concentrations as reflected by the experimental results shown in Fig. 1. We want to employ the model to give one possible explanation of the different oil recovery curves.

Initially the core is assumed to be preferentially oil-wet and represented by the relative permeability and capillary pressure function $k(s, \rho_{c,0}) = k^{ow}(s)$, $k_o(s, \rho_{c,0}) = k_o^{ow}(s)$, and $P_c(s, \rho_{c,0}) = P_c^{ow}(s)$ shown in Fig. 3. All the simulations are for a constant initial saturation $s_0(x) = 0.191$ which corresponds approximately to the value where $P_c^{ow}(s) = 0$. In other words, practically speaking, no water will imbibe into the core for this wetting state, as will be demonstrated below. The other extreme is that the core plug initially is assumed to be water-wet. This will give a

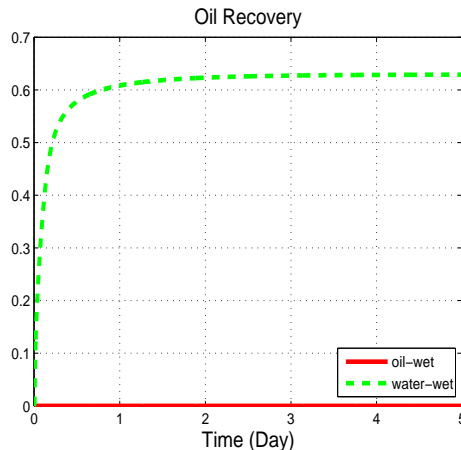


FIGURE 5. Oil recovery curves for EF-0 (see Table 2 in Appendix A) as imbibing fluid and with, respectively, a fixed preferentially oil-wet and water-wet core.

maximal oil recovery, independent of the brine composition. These two extremes are illustrated in Fig. 5.

However, we are interested in the case where the brine composition has a potential to *change* the wetting state. In other words, if the brine composition of the fluid which surrounds the core is different from the one inside the core, ionic concentration fronts will be formed that move through the open faces of the core due to molecular diffusion. This creates a non-equilibrium state regarding the water-rock chemistry that in turn will trigger dissolution/precipitation processes. This implies a change in the wetting state towards a more water-wet surface at the places inside the core where dissolution of calcite takes place. As a result, capillary forces will then drive water into the core at these places. Below we will consider a series of different brine compositions for the imbibing fluid. These compositions are directly related to those used in the experimental work [47] and corresponds to the results shown in Fig. 1.

- Example 1: First we apply EF-0 as the imbibing fluid for a period of 15 days with fixed wetting state;
- Example 2a: Then, seawater-like brines without Ca^{2+} and Mg^{2+} ions referred to as Sw0x0S, Sw0x1S, Sw0x2S, Sw0x4S are employed as imbibing fluid for a period of 15 days, see Table 2 in Appendix A;
- Example 2b: This is a continuation of Example 2, however, a seawater like concentration of Mg^{2+} is now added to the brines Sw0x0S, Sw0x1S, Sw0x4S whereas a seawater like concentration of Ca^{2+} is added to the brine Sw0x2S. We refer to Table 3 in Appendix A for details of the brine compositions.
- Example 3: The purpose of this example is to test the effect of increasing the CO_2 partial pressure.
- Example 4: Test of grid refinement.

It is assumed that the core initially is filled with formation water EF-0 in the pore space. The core is composed of calcite only. Before we start the imbibition process we make sure that the formation water reaches its equilibrium state with calcite, i.e., we solve the RD model forward in time until a steady state is reached. This introduces a small modification of the ion concentrations. It's important to note that for all the numerical experiments carried out in the following examples we use the same set of parameters as described in detail in Appendix A and B (molecular diffusion, capillary pressure, reaction rate coefficients, etc). Hence, the only change from one case to another is the *brine composition*. In order to focus on capillary forces only we will also neglect gravity in the following computations.

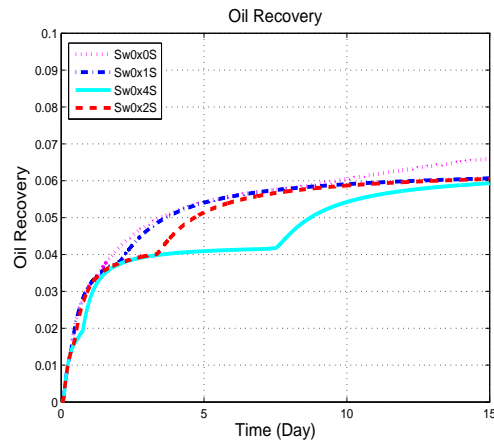


FIGURE 6. Plots showing the oil recovery for the different seawater-like brines without Ca^{2+} and Mg^{2+} ions referred to as Sw0x0S, Sw0x1S, Sw0x2S, Sw0x4S, see Table 2 in Appendix A, during the first 15 days.

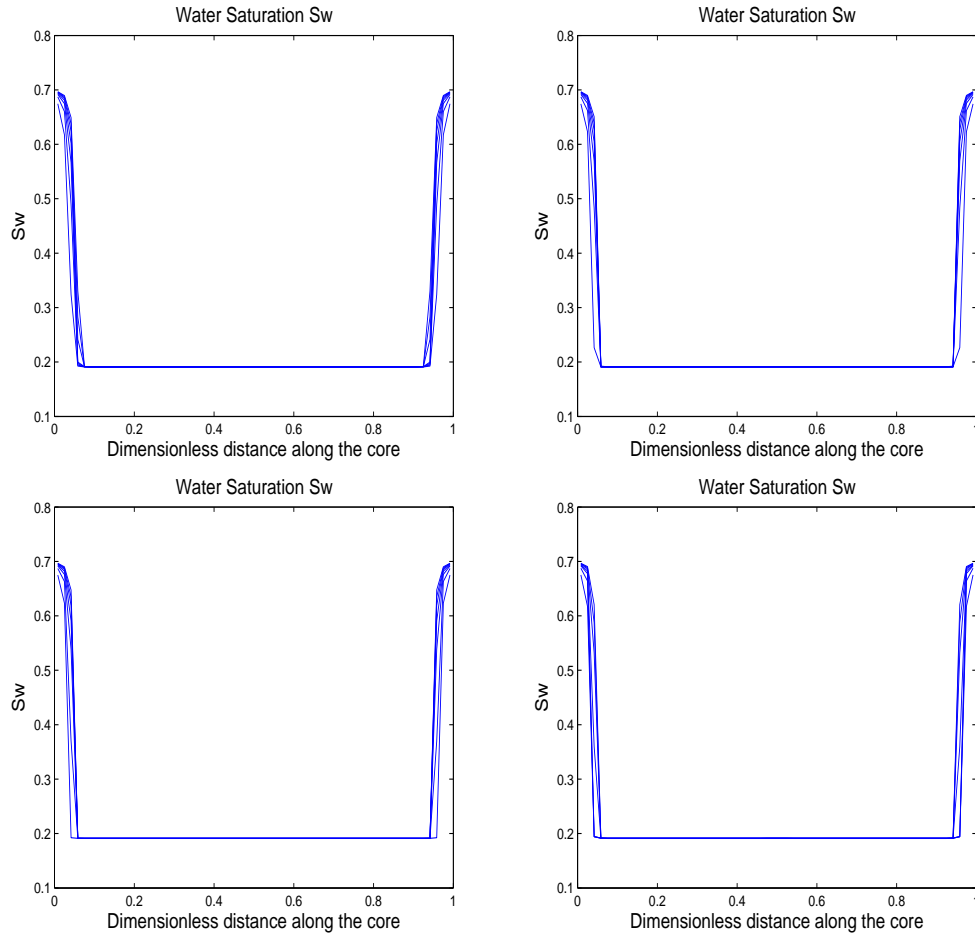


FIGURE 7. Plots showing the water saturation distribution inside the core during the first 15 days that correspond to the different oil recovery curves in Fig. 6. **Top** (left): Sw0x0S. **Top** (right): Sw0x1S. **Bottom** (left): Sw0x2S. **Bottom** (right): Sw0x4S.

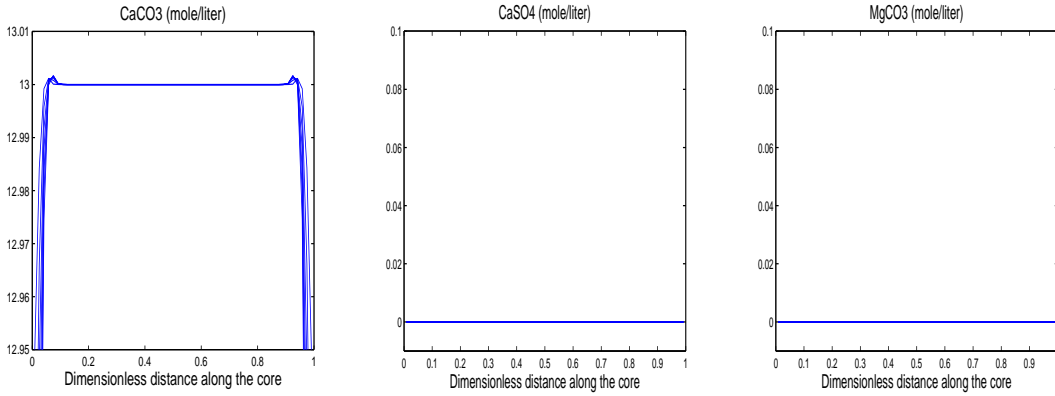


FIGURE 8. Plots showing the changes in the mineral composition during the first 15 days for the brine Sw0x1S. **Left:** CaCO_3 . **Middle:** CaSO_4 . **Right:** MgCO_3 . There is a small dissolution of calcite that takes place near the outlet ends due to the fact that the imbibing brine (Sw0x1S) has a different composition compared to the brine initially in the core (EF-0). This generates a corresponding change in the wetting state towards a more water-wet surface in the region where dissolution of calcite takes place, consequently, water is imbibed as reflected by Fig. 7 (bottom, right figure). However, the dissolution front only moves a small distance into the core for this brine. In particular, there is no precipitation of anhydrite or magnesite.

5.1. Example 1: Formation water (EF-0) as the imbibing fluid with fixed wetting states. We study the effect of using the EF-0 brine as the imbibing fluid and with a fixed wetting state. Firstly, we assume the core is preferentially oil-wet and represented by the oil-wet relative permeability and capillary pressure functions $k^{ow}(s)$, $k_o^{ow}(s)$, and $P_c^{ow}(s)$. Secondly, we assume the core is water-wet and represented by the water-wet relative permeability and capillary pressure functions $k^{ww}(s)$, $k_o^{ww}(s)$, and $P_c^{ww}(s)$. The corresponding oil recovery curves are shown in Fig. 5 indicating, as expected, that no water will imbibe into the core when it is oil-wet whereas the oil-recovery is strong for the water-wet case. These two extremes set the stage for exploring brine-dependent spontaneous imbibition.

5.2. Example 2: Brines without Ca^{2+} and Mg^{2+} but various SO_4^{2-} concentration. In this example we study the spontaneous imbibition behavior for the four seawater-like brines without Ca^{2+} and Mg^{2+} ions respectively referred to as Sw0x0S, Sw0x1S, Sw0x2S, Sw0x4S.

a) Period 1:0-15 days. The various oil recovery curves are shown in Fig. 6 whereas the saturation distribution inside the core for the different brines at increasing times are shown in Fig. 7. Corresponding mineral distributions inside the core for calcite, anhydrite, and magnesite are shown in Fig. 8 for the brine Sw0x1S. Similar behavior is observed for three other brines Sw0x0S, Sw0x2S, and Sw0x4S (plots are not included). Main observations are:

- Using Sw0x1S (or some of the other seawater like brines) as the imbibing fluid means that there will be concentration fronts that diffuse through the open faces creating a non-equilibrium state in a mixing zone inside the core. The water-rock system will move towards a new equilibrium state that involve a balance between transport and dissolution/precipitation corresponding to Fig. 8. In particular, associated with this new equilibrium state there is a very slowly moving calcite dissolution front and a corresponding wettability alteration behind this front.
- The experimental oil recovery for the four different brines Sw0x0S, Sw0x1S, Sw0x2S, and Sw0x4S shown in Fig. 1 reflect a very low oil recovery which is most likely due to fluid expansion and/or inhomogeneities in the wetting conditions [47]. In other words, these

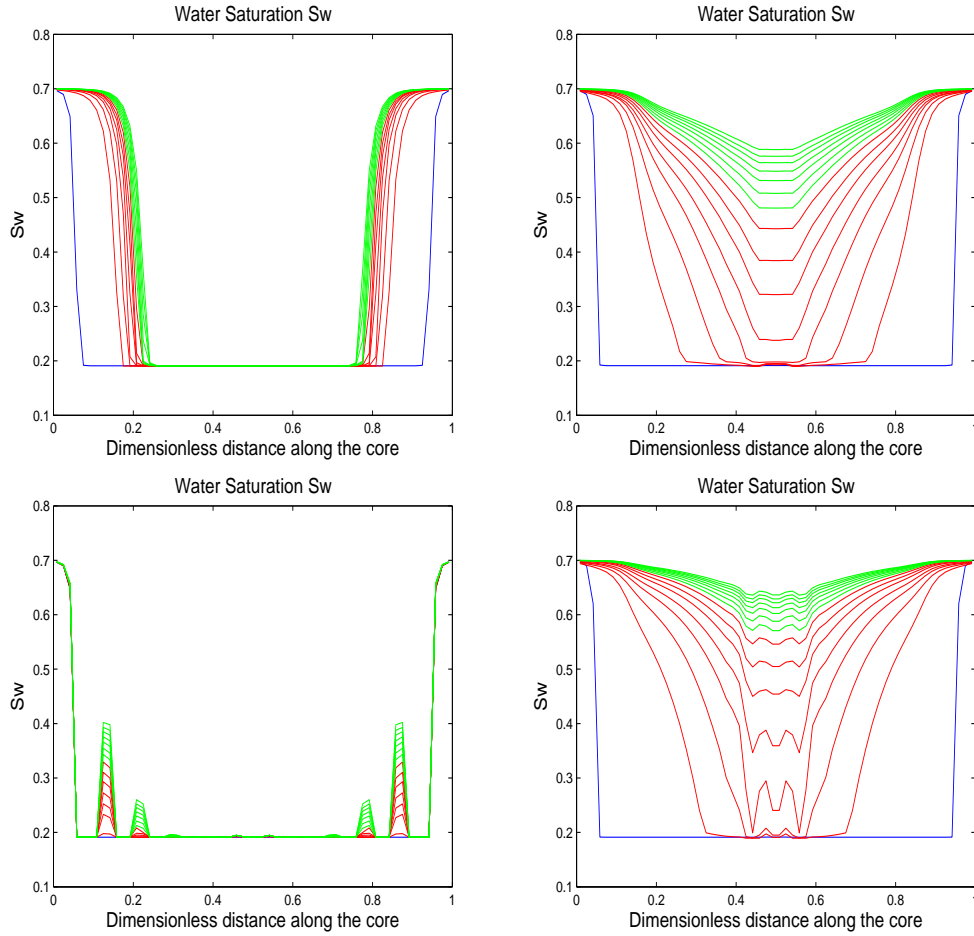


FIGURE 9. This plot is a natural continuation of Fig. 7. The plots show the water saturation distribution inside the core during the next 30 days (15-30 days=red, 30-45 days=green) after the brine has been altered by adding Mg^{2+} or Ca^{2+} . **Top (left):** $Sw0x0S + 1Mg^{2+}$. **Top (right):** $Sw0x1S + 1Mg^{2+}$. **Bottom (left):** $Sw0x2S + 1Ca^{2+}$. **Bottom (right):** $Sw0x4S + 1Mg^{2+}$.

brine compositions to a minor degree trigger a change of the wetting state in line with the model predictions.

b) Period 2:15-45 days: The impact of adding Mg^{2+} or Ca^{2+} ions to the imbibing fluid. The purpose of this experiment, which is a natural continuation of the previous example, is to investigate along the same line as the experiments shown in Fig. 1, what happens when we add a seawater like concentration of Mg^{2+} ions to the brines $Sw0x0S$, $Sw0x1S$, and $Sw0x4S$ whereas we add a seawater like concentration of Ca^{2+} to the brine $Sw0x2S$. Main observations in view of Fig. 9 and Fig. 10 are:

- Adding Mg^{2+} to $Sw0x0S$ gives a new (dynamic) equilibrium state associated with the water-rock system which implies that the calcite dissolution front moves further into the core generating a corresponding change of wetting state (see top row of Fig. 10). However, the speed of this dissolution front gradually decreases thereby giving a moderate water front displacement (see top-left of Fig. 9) and corresponding oil recovery (see Fig. 2).
- However, if SO_4^{2-} is present (as in brine $Sw0x1S$ and $Sw0x4S$) the dissolution of calcite will move deeper into the core (see second and fourth row of Fig. 10) giving a much more efficient water imbibition (see top-right and bottom-right of Fig. 9). The corresponding

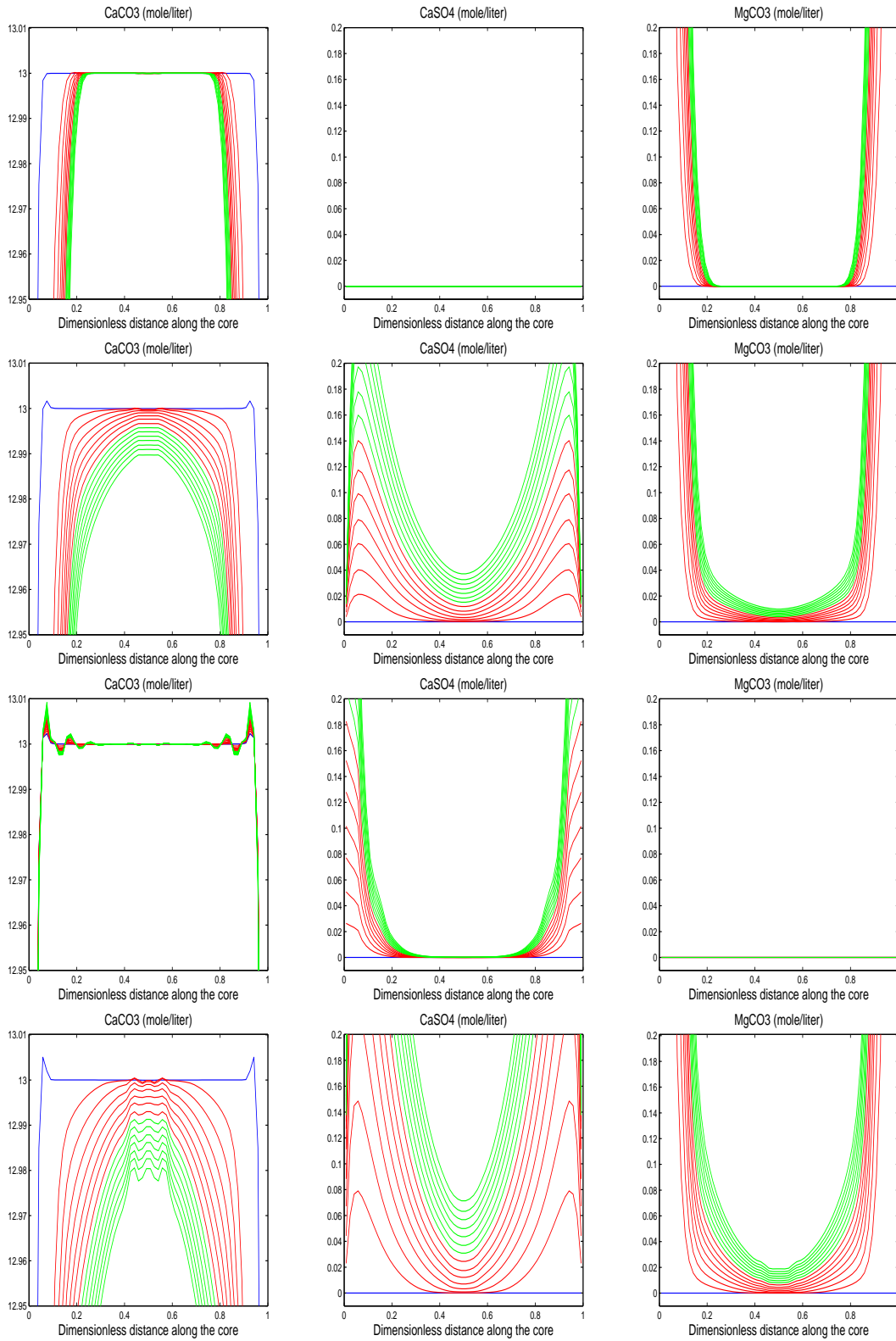


FIGURE 10. Plots showing the changes in the mineral composition during the period 15-45 days (15-30 days=red, 30-45 days=green). **First row:** $\text{Sw}0\text{x}0\text{S} + 1\text{Mg}^{2+}$. **Second row:** $\text{Sw}0\text{x}1\text{S} + 1\text{Mg}^{2+}$. **Third row:** $\text{Sw}0\text{x}2\text{S} + 1\text{Ca}^{2+}$. **Fourth row:** $\text{Sw}0\text{x}4\text{S} + 1\text{Mg}^{2+}$.

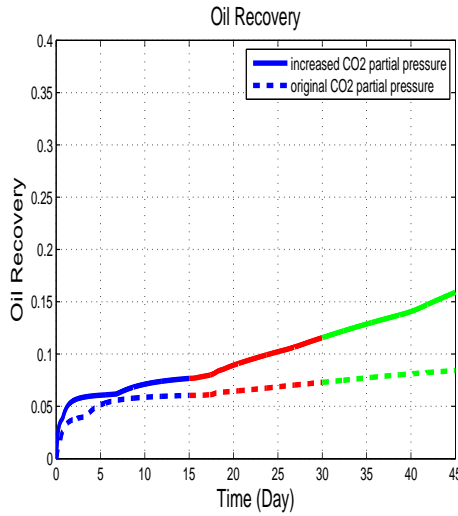


FIGURE 11. The plots show how the model is sensitive for the CO_2 partial pressure. The brine $\text{Sw}0 \times 2\text{S}$ (with added Ca^{2+} after 15 days) is considered for two different values of the CO_2 partial pressure. Higher CO_2 partial pressure gives a stronger change of the wetting state and more oil is produced.

oil recovery curves shown in Fig. 2 give a behavior similar to the experimental curves in Fig. 1.

- Adding Ca^{2+} to $\text{Sw}0 \times 2\text{S}$ gives a somewhat different and possible interesting behavior. For this brine composition the water-rock chemistry model will suggest a situation where dissolution and precipitation of calcite will appear successively as we move into the core (see third row of Fig. 10). This in turn gives rise to a non-uniform water front behavior (since the change of the wetting state towards a more water-wet surface will spread in a non-uniform manner). In [46] is included a picture showing the oil distribution inside a core after a spontaneous imbibition experiment. The imbibing brine is a seawater like brine with high concentration of SO_4^{2-} , and interestingly enough it demonstrates that oil has been released in a highly non-uniform manner.

The oscillatory behavior seen for the calcite concentration naturally rise the question: Is this a numerical instability or a "physical instability"? There are many examples from the literature that the combined effect of diffusion and chemical reactions can give rise to oscillatory behavior. Some well known examples are Liesegang rings and Brusselator systems [16, 17, 18]. For example, Liesegang phenomena is a result of the interaction of diffusion of ions with precipitation reaction between them. It turns out that this can create inhomogeneous distribution of formed precipitate. Under the right circumstances, precipitation bands are formed according to a special spacing regularity. Currently there is a considerable activity within this field, both from an experimental point of view as well as modeling [16]. Similarly, a Brusselator system involves nonlinear coupling between reactions and diffusion of ions which give rise to chemical oscillations in time and space [17]. Since our model is given as a strongly coupled and nonlinear system of diffusion-reaction equations, it is not unlikely that the nonhomogeneous precipitation shown in Fig. 10 can be a result of intrinsic properties of the model itself and not numerical instability. On the other hand, the numerical approach we rely on is a splitting approach where we alternate between solving the chemical reaction part and the transport part. This approach is often used to solve transport-reaction models. See for example references like [25] (Chapter 2). But it is also known that this approach occasionally show numerically unstable behavior depending on the problem considered. However, it is beyond the scope of this work to explore this in detail.

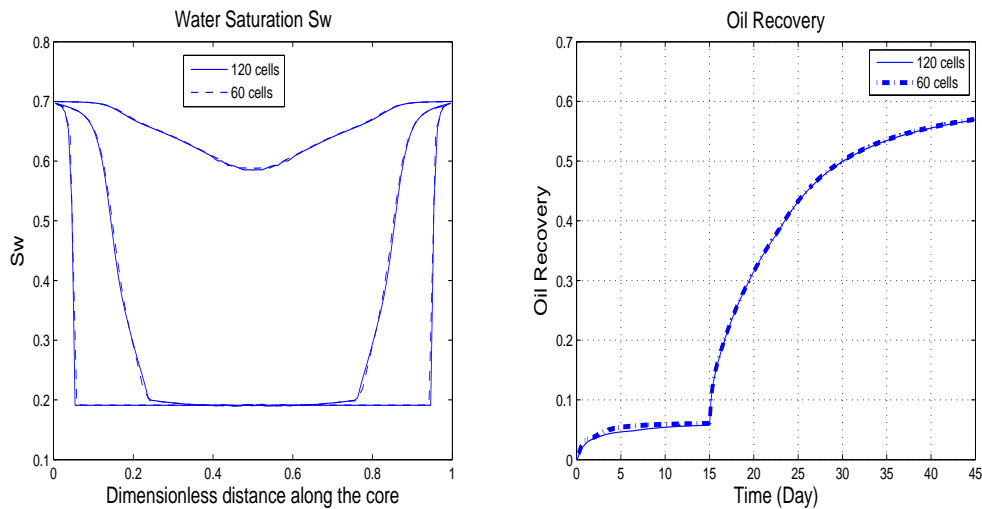


FIGURE 12. Convergence test for the problem with the brine Sw0x1S. We have computed solutions at two grids corresponding to 60 and 120 cells. **Left:** Saturation distribution at different times during the period 0-45 days. **Right:** Oil recovery curves.

5.3. Example 3: The effect of changing the CO₂ partial pressure. The purpose of this example is to explore the model behavior when we increase the CO₂ partial pressure constant P_{CO_2} . This implies that more CO₂ is dissolved in the brine (carbonated water). As an example we consider the case with the brine Sw0x2S where we add Ca²⁺ after 15 days. Changing the P_{CO_2} constant from $10^{-3.5}$ bar to $10^{-0.5}$ bar implies that the pH is lowered from 5.96 to 4.62. As a consequence the brine becomes more reactive, which impacts the dissolution of calcite, and finally the change of the wetting state. The resulting oil recovery curve is shown in Fig. 11 and reflects that more water will imbibe for the carbonated water. We may refer to the interesting work [42] for an experimental study of the role played by pH for spontaneous counter-current imbibition, though in a different context.

5.4. Example 4: Convergence test. Finally, in this example we have refined the grid for the case with the brine Sw0x1S (with added Mg²⁺ after 15 days). For the previous calculations we have used a grid of 60 cells and a time splitting step between transport and reaction corresponding to 3 minutes. We also compute solutions for the brine Sw0x1S by using a grid of 120 cells and the same number of splitting steps. Results are shown in Fig. 12 indicating that the numerical solution converges reasonable well. Note that the model is quite demanding to solve. It takes approximately 2.5 hours to simulate on a grid of 60 cells a 15 days lab experiment on a standard PC (HP Intel(R) Core(TM)2 Duo CPU, 2.99 GHz, 3.46 GB RAM). Moreover, it takes approximately 7 hours to simulate the same case on a grid of 120 cells.

6. CONCLUDING REMARKS

We have explored a model relevant for spontaneous imbibition experiments where the oil recovery is sensitive to the brine composition. The model has been designed for studying the role of important ions like Ca²⁺, Mg²⁺, and SO₄²⁻ for chalk cores. The main idea is to couple a RD system for the water-rock chemistry with the saturation equation. More precisely, the wetting state represented through the flow functions (relative permeability and capillary pressure) is linked to the water-rock chemistry such that a change towards a more water-wet surface appears at the places where dissolution of calcite takes place. The dissolution of calcite is clearly sensitive to the brine composition. Consequently, the model will predict brine-dependent oil recovery curves. Some main observations are:

- (i) The model will, for a fixed set of parameters, capture main trends of the experimental results shown in Fig. 1.
- (ii) In particular, the model gives a possible interpretation of the experimental observation that increasing concentration of SO_4^{2-} , if Mg^{2+} is present in the brine, gives the most efficient oil recovery.
- (iii) The brine-dependent oil recovery is clearly demonstrated. The brine composition will determine to what extent and where dissolution of calcite will take place, and thereby the corresponding wettability alteration towards more water-wet regions, inside the core.
- (iv) We have also observed that the model can suggest a range of different scenarios depending on the brine composition. In particular, non-uniform water front displacement and sensitivity for the CO_2 partial pressure were observed.

The work presented here is subject to a number of possible interesting further investigations:

- (i) More systematic studies of simplified versions of the proposed model. In particular, it would be interesting to derive a simpler version of it that still can give solutions similar to those that were observed. More insight into the coupling mechanisms between the RD model and the BL model is necessary, in particular, try to identify how and why the model can predict nonuniform water front displacement.
- (ii) Investigations of how to solve the proposed model more efficiently from a computational point of view. It has been observed that the model is challenging to solve accurately (depending on the brine composition) and hence motivates for finer investigations of these aspects.
- (iii) The observations of the model behavior can also serve as a motivation for new lab experiments where the experimental setup is chosen to be consistent with the model. For example, we will consider core plugs that are sealed everywhere except at the two ends making the lab experiments essentially one-dimensional. An interesting issue then, in view of the behavior predicted by the model, is to study how and where inside the core oil will be released as a function of the brine composition.
- (iv) Consider other possible coupling mechanisms between water-rock chemistry and two-phase flow functions. For instance, can the observed behavior in terms of oil recovery be explained by surface chemistry instead of dissolution/precipitation?

REFERENCES

- [1] C.A.J. Appelo and D. Postma, *Geochemistry, groundwater and pollution*, Taylor & Francis Group, 2009.
- [2] D. Aregba-Driollet, F. Diele, and R. Natalini, A mathematical model for the sulphur dioxide aggression to calcium carbonate stones: Numerical approximation and asymptotic analysis, *SIAM J. Appl. Math.* **64** (5), 1636–1667, 2004.
- [3] T. Austad and D.C. Standnes Wettability and Oil recovery from Carbonates: Effects of Temperature and Potential Determining Ions, *Journal of Petroleum Science and Engineering*, **39**, 363–376, 2003.
- [4] G.I. Barenblatt, V.M. Entov, V.M. Ryzhik, *Theory of Fluid Flows Through Natural Rocks*, Kluwer Academic Publisher, 1990.
- [5] G.I. Barenblatt, T.W. Patzek, V.M. Prostokishin, and D.B. Silin, SPE75230: Oil deposit in diatomites: A new challenge for subterranean mechanics, SPE/DOE Improved Oil Recovery Symposium, 2002.
- [6] J. Bear, *Dynamics of Fluids in Porous Media*, Elsevier, Amsterdam, 1972.
- [7] N. Bouillard, R. Eymard, R. Herbin, and P. Montarnal, Diffusion with dissolution and precipitation in a porous medium: mathematical analysis and numerical approximation of a simplified model, *ESAIM: M2AN* **41**(6), 975–1000, 2007.
- [8] N. Bouillard, R. Eymard, M. Henry, R. Herbin, and D. Hilhorst, A fast precipitation and dissolution reaction for a reaction-diffusion system arising in a porous medium, *Nonlinear Analysis: Real World Applications* **10**, 629–638, 2009.
- [9] D. Boyd, K. Al Nayadi, et al. *Validating laboratory measured archie saturation exponents using non-resistivity based methods*, Paper prepared for presentation at the Society of Core Analysts held in Abu Dhabi, UAE, 5-9 October 2004.
- [10] L.M. Cathles, EQAlt–Equilibrium Chemical Alteration. Combined Physical and Chemical Geofluids Modeling, University of Windsor, Windsor, Ontario, 2006.
- [11] Z. Chen, G. Huan, and Y. Ma, *Computational Methods for Multiphase Flows in Porous Media*, SIAM Computational Science & Engineering, Philadelphia, 2006.

- [12] J.-S. Chen and C.-W. Liu, *Numerical simulation of the evolution of aquifer porosity and species concentrations during reactive transport*, *Computers & Geosciences*, **28** (2002), 485–499.
- [13] C. J. van Duijn and M. J. de Neef, Similarity solution for capillary redistribution of two phases in a porous medium with a single discontinuity. *Adv. Water Resources*, **21**, pp. 451-461, 1998.
- [14] S. Evje, A. Hiorth, M.V. Madland, R. Korsnes, A mathematical model relevant for weakening of chalk reservoirs due to chemical reactions, *Networks and Heterogeneous Media*, **3** (2009), 149–183.
- [15] S. Evje and A. Hiorth, A mathematical model for dynamic wettability alteration controlled by water-rock chemistry, *Networks and Heterogeneous Media*, **5** (2010), 217–256.
- [16] B.A. Grzybowski, *Chemistry in motion*, Wiley, UK, 2009.
- [17] E. Hairer and G. Wanner, *Solving Ordinary Differential Equations II, Stiff and Differential-Algebraic Problems*, Springer-Verlag, Berlin, 1991.
- [18] D. Hilhorst, R. van der Hout, M. Mimura, and I. Ohnishi, A mathematical study of the one-dimensional Keller and Rubiñow model for Liesegang Bands, *J. Stat. Phys.* **135**, 107–132, 2009.
- [19] A. Hiorth, L.M. Cathles, J. Kolnes, O. Vikane, A. Lohne, and M.V. Madland, A chemical model for the seawater-CO₂-carbonate system – aqueous and surface chemistry, Paper prepared for presentation at the Wettability Conference held in Abu Dhabi, UAE, 27–28 october, 2008.
- [20] A. Hiorth, L.M. Cathles, and M.V. Madland, *The impact of pore-water chemistry on carbonate surface charge and oil wettability*, *Transport Porous Media*, to appear, 2010.
- [21] G.R. Jerauld, C.Y. Lin, K.J. Webb, and J.C. Secombe, *Modeling Low-Salinity Waterflooding*, *SPE Reservoir Evaluation & Engineering*, **11** (2008), 1000-1012.
- [22] R. Juanes, Nonequilibrium effects in models of three-phase flow in porous media, *Adv. Water Res.* **31**, 661–673, 2008.
- [23] D. Kashchiev and A. Firoozabadi, Analytical solutions for 1D countercurrent imbibition in water-wet media, *SPE Journal* **8** (4), 401-408, 2003.
- [24] R.I. Korsnes, M.V. Madland, T. Austad, S. Haver, and G. Røesland, The effects of temperature on the water weakening of chalk by seawater, *J. Pet. Sci. Eng.* **60**(3-4), 183-193, 2008.
- [25] P.C. Lichtner, C.I. Steefel, and E.H. Oelkers, Reactive transport in porous media, *Reviews in Mineralogy*, **34**, Mineralogical Society of America, Washington D.C., 1996.
- [26] A.C. Lasaga, *Kinetic Theory in the Earth Sciences, Princeton series in geochemistry*, Princeton University Press, 1998.
- [27] S.S. Le Guen and A.R. Kovalscek, Nonequilibrium effects during spontaneous imbibition, *Transport Porous Media*, **63** (2006), 127–146.
- [28] R.J. LeVeque, *Finite Volume Methods for Hyperbolic Problems*, Cambridge Texts in Applied Mathematics, Berlin, 2002.
- [29] M.V. Madland, A. Hiorth, E. Omdal, M. Megawati, T. Hildebrand-Habel, R.I. Korsnes, S. Evje, L.M. Cathles, Chemical alterations induced by rock-fluid interactions when injecting brines in high porosity chalks, *Transport Porous Media* **87**, 679-702, 2011.
- [30] M.V. Madland, A. Finsnes, A. Alkafadgi, R. Risnes, and T. Austad, The influence of CO₂ gas and carbonate water on the mechanical stability of chalk, *J. Pet. Sci. Eng.* **51**, 149-168, 2006.
- [31] J.W. Morse and R.S. Arvidson, The dissolution kinetics of major sedimentary carbonate minerals, *Earth-Science Reviews*, **58** (2002), 51–84.
- [32] D.A. Nield and A. Bejan, *Convection in Porous Media*, Springer Verlag, 1992.
- [33] M. Pooladi-Darvish and A. Firoozabadi, Cocurrent and countercurrent imbibition in a water-wet matrix block, *Soc. Petrol. Engng. J.*, **5** (2000), 3–11.
- [34] J.M. Schembre, G.-Q. Tang, and A.R. Kovalscek, Wettability alteration and oil recovery by water imbibition at elevated temperatures, *J. Pet. Sci. Eng.*, **52** (2006), 131–148.
- [35] J.M. Schembre and A.R. Kovalscek, Estimation of dynamic relative permeability and capillary pressure from countercurrent imbibition experiments, *Transport Porous Media*, **65** (2006), 31–51.
- [36] D. Silin and T. Patzek, On Barenblatt’s model of spontaneous countercurrent imbibition, *Transport Porous Media*, **54** (2004), 297–322.
- [37] D.C. Standnes, T. Austad, Wettability alteration in chalk 2. Mechanism for wettability alteration from oil-wet to water-wet using surfactants, *J. Pet. Sci. Eng.*, **28**, 123–143, 2000.
- [38] Skule, Strand., D.C. Standnes, T. Austad, Spontaneous imbibition of aqueous surfactant solutions into neutral to oil-wet carbonate cores: Effects of brine salinity and composition, *Energy and Fuels*, **17**, 1133–1144, 2000.
- [39] D.C. Standnes, T. Austad, Wettability alteration in carbonate interaction between cationic surfactant and carboxylates as a key factor in wettability alteration from oil-wet to water-wet conditions, *Colloids and Surfaces A: Physicochem. Eng. Aspects*, **216**, 243–259, 2003.
- [40] C.I. Steefel and A.C. Lasaga, A coupled model for transport of multiple chemical species and kinetic precipitation/dissolution reactions with application to reactive flow in single phase hydrothermal systems, *American J Sci.*, **294** (1994), 529–592.
- [41] S. Strand, E.J. Høegnesen, T. Austad, Wettability alteration of carbonates Effects of potential determining ions (Ca²⁺ and SO₄²⁻) and temperature, *Colloids and Surfaces A: Physicochem. Eng. Aspects*, **275**, 1–10, 2006.
- [42] S. Takahashi and A.R. Kovalscek, Spontaneous countercurrent imbibition and forced displacement characteristics of low-permeability, siliceous shale rock, *J. Pet. Sci. Eng.* **71** (2010), pp. 47–55.

- [43] I. Tripathi and K.K. Mohanty, Instability due to wettability alteration in displacements through porous media, *Chemical Eng. Sci.*, **63** (2008), 5366–5374.
- [44] L. Yu, S. Evje, I.Fjelde, H. Kleppe, T. Kaarstad, and S.M. Skjaeveland, Modelling of wettability alteration processes in carbonate oil reservoirs, *Networks and Heterogeneous Media*, **3** (2008), 149–183.
- [45] L. Yu, S. Evje, I.Fjelde, H. Kleppe, T. Kaarstad, and S.M. Skjaeveland, Spontaneous Imbibition of Seawater into Preferentially Oil-Wet Chalk Cores - Experiments and Simulations, *J. Pet. Sci. Eng.*, **66** (2009), pp. 171-179.
- [46] P. Zhang and T. Austad, Wettability and Oil recovery from Carbonates: Effects of Temperature and Potential Determining Ions, *Colloids and Surfaces A: Physicochem. Eng. Aspects*, **279**, 179–187, 2006.
- [47] P. Zhang, M.T. Tweheyo, T. Austad, Wettability alteration and improved oil recovery by spontaneous imbibition of seawater into chalk: Impact of the potential determining ions Ca²⁺, Mg²⁺, and SO₄²⁻, *Colloids and Surfaces A: Physicochem. Eng. Aspects*, **301**, 199–208, 2007.

APPENDIX A: DATA FOR WATER-ROCK CHEMISTRY

Activity coefficients. According to the Debye-Hückel equation, see for example [26, 1], the activity coefficient γ_i is given by

$$-\log_{10}(\gamma_i) = \frac{AZ_i^2\sqrt{I_0}}{1 + a_i^0 B\sqrt{I_0}}, \quad (51)$$

where the index i refers to the different species involved in the system which is studied. Moreover, Z_i refers to the ionic charges, $A(T)$ and $B(T)$ are temperature dependent given functions, similarly for the constants a_i^0 , whereas I_0 refers to the ionic strength defined by

$$I_0 = \frac{1}{2} \sum_i C_i Z_i^2. \quad (52)$$

For the numerical calculations, we calculate I_0 based on the ion concentrations for the imbibing brine. Since the temperature is kept constant, the activity coefficients are also taken to be constant, according to (51).

As commented in [1] the Debye-Hückel equation (51) is limited to $I_0 < 0.1$. Various equations have been proposed to derive activity coefficients at higher ionic strength than 0.1. One such variant of the Debye-Hückel equation is due to Truesdell and Jones and takes the following form, see [1] and references therein for more details,

$$\log_{10}(\gamma_i) = -\frac{AZ_i^2\sqrt{I_0}}{1 + a_i B\sqrt{I_0}} + b_i I_0, \quad (53)$$

where a_i and b_i are ion-specific fit parameters. Note that a_i in (53) is different from a_i^0 in (51) whereas A and B are the same parameters. Since the brines we consider have ionic strength higher than 0.1 we shall apply the Truesdell and Jones correlation. The following values, taken from [1], are used for the constants a_i, b_i in (53):

i	a_i	b_i
h	4.78	0.24
oh	10.65	0.21
co	5.4	0
ca	5	0.165
hco	5.4	0
na	4	0.075
cl	3.5	0.015
mg	5.5	0.20
so	5	-0.04

Moreover, we shall use the following values for $A(T)$ and $B(T)$ taken from [10, 19]:

$$A(T = 130) = 0.6623, \quad B(T = 130) = 0.3487. \quad (54)$$

	T=25	T=70	T=90	T=130
K^c	$10^{+1.86}$	$10^{+1.21}$	$10^{+0.92}$	$10^{+0.35}$
K^g	$10^{-4.3}$	$10^{-4.87}$	$10^{-5.21}$	$10^{-5.94}$
K^m	$10^{+2.3}$	$10^{+1.24}$	$10^{+0.79}$	$10^{-0.01}$
K	$10^{-7.87}$	$10^{-8.05}$	$10^{-8.33}$	$10^{-9.01}$
C_w	$10^{-14.05}$	$10^{-12.72}$	$10^{-12.47}$	$10^{-12.26}$
C_2	$10^{-10.32}$	$10^{-10.09}$	$10^{-10.08}$	$10^{-10.15}$

TABLE 1. Equilibrium constants relevant for the chemical reactions (2)–(4) and (15)–(17).

Ions	EF-0 [mol/l]	SW [mol/l]	SW0x0S [mol/l]	SW0x1S [mol/l]	SW0x2S [mol/l]	SW0x4S [mol/l]
Na^+	1.452	0.459	0.647	0.631	0.607	0.559
Cl^-	1.452	0.527	0.647	0.583	0.511	0.367
Ca^{2+}	0	0.013	–	–	–	–
Mg^{2+}	0	0.045	–	–	–	–
SO_4^{2-}	0	0.024	–	0.024	0.048	0.096
Ion Strength I_0	1.452	0.657	0.647	0.655	0.655	0.655
pH	6.06	5.95	5.95	5.95	5.95	5.95

TABLE 2. Composition of different brines used in the first time period (0-15 days) before adding Ca^{2+} or Mg^{2+} .

Ions	SW0x0S+1Mg ²⁺ [mol/l]	SW0x1S+1Mg ²⁺ [mol/l]	SW0x2S+1Ca ²⁺ [mol/l]	SW0x4S+1Mg ²⁺ [mol/l]
Na^+	0.647	0.631	0.607	0.559
Cl^-	0.647 + 0.090	0.583 + 0.090	0.511 + 0.026	0.367 + 0.090
Ca^{2+}	–	–	0.013	–
Mg^{2+}	0.045	0.045	–	0.045
SO_4^{2-}	–	0.024	0.048	0.096
Ion Strength I_0	0.782	0.790	0.694	0.790
pH	5.97	5.97	5.96	5.97

TABLE 3. Composition of the different brines where we add seawater concentration of Mg^{2+} to the brines SW0x0S, SW0x1S, and SW0x4S respectively (by adding MgCl_2), and seawater concentration of Ca^{2+} to the brine SW0x2S (by adding CaCl_2).

Equilibrium constants. The following equilibrium constants are used: K^c , K^g , K^m refer to (19)–(22), K refer to (5), C_2 refer to (6), and C_w to (7). In order to calculate C_1 in (5), we have used the given K value from Table 1 and the CO_2 partial pressure P_{CO_2} constant is set to $P_{\text{CO}_2} = 10^{-3.5}$ bar. All these constants have been taken from the EQAlt-simulator [10, 19].

Brine compositions. In Table 2 we specify brines relevant for the imbibition process during the first 15 days. In Table 3 we specify the brines used after 15 days where, respectively, Ca^{2+} or Mg^{2+} has been added.

Core properties. The following core properties are assumed for the model example studied below.

Act coeff	γ_{ca}	γ_{so}	γ_{mg}	γ_{na}	γ_{cl}	γ_h	γ_{oh}	γ_{co}	γ_{hco}
EF-0	0.1622	0.0817	0.2120	0.6474	0.4998	1.2112	1.4426	0.1056	0.5700
SW0x0S	0.1659	0.1222	0.1956	0.6273	0.5507	0.8466	1.0052	0.1421	0.6140
SW0x1S	0.1655	0.1215	0.1954	0.6271	0.5497	0.8492	1.0086	0.1414	0.6132
SW0x2S	0.1655	0.1215	0.1954	0.6271	0.5497	0.8492	1.0086	0.1414	0.6132
SW0x4S	0.1655	0.1215	0.1954	0.6271	0.5497	0.8492	1.0086	0.1414	0.6132

TABLE 4. Activity coefficients for some of the brines.

- Length: $L = 0.04$ m
- Porosity: $\phi = 0.4$
- Volume of core: $V_c = 75$ ml
- Volume of matrix: $V_m = 45$ ml
- Mass of rock: $M_c = 100$ g
- Permeability: $\kappa = 5$ mD = $5 \cdot 0.987 \cdot 10^{-15}$ m².

In view of the fact that the molecular weight of CaCO₃ is 100g/mol, it follows that the solid part of the core corresponds to 1 mol CaCO₃. Consequently, the molar density is $\rho_c = 1/V_c$ mol/liter \approx 13 mol/liter.

Oil properties.

- Oil viscosity: $\mu_o = 0.6$ cp (1 cp = 10^{-3} Pa s)
- Oil density : $\rho_o = 0.73$ g/cm³

Brine properties.

- Water viscosity: $\mu = 0.3$ cp
- Water density: $\rho = 0.92$ g/cm³.

Other quantities.

- Reference molecular diffusion: $\bar{D}_m = 5 \cdot 10^{-9}$ m²/s.
- We use $p = q = 1.9$ in the expression (36).
- Reference capillary pressure: $\bar{P}_c = 2 \cdot 10^4$ Pa.
- Reference viscosity: $\bar{\mu} = 10^{-3}$ Pa s.

Oil recovery is defined as

$$\text{Oil Recovery} := \frac{\int_0^1 [s(x, t) - s_{\text{init}}(x)] dx}{\int_0^1 [1 - s_{\text{init}}(x)] dx},$$

where $s_{\text{init}}(x)$ is initial water saturation in the core.

Reaction rate constants. The reaction rate constants are set as follows:

$$k_1^c = 1.5 \cdot 10^{-5}, \quad k_1^g = 0.001k_1^c, \quad \text{and} \quad k_1^m = 0.4k_1^c \quad (\text{in terms of (mol/liter)}). \quad (55)$$

These parameters are kept constant for all simulations.

APPENDIX B: DATA FOR WATER-OIL FLOW FUNCTIONS

Oil-wet conditions. The following set of values for preferentially *oil-wet* conditions is used:

$$k_o^{*,ow} = 0.7, \quad k_o^{*,ow} = 0.75, \quad s_{wr}^{ow} = 0.1, \quad s_{or}^{ow} = 0.15, \quad Nk_o^{ow} = 2, \quad Nk_o^{ow} = 3. \quad (56)$$

Applying these values in (27) the following two sets of relative permeability curves are obtained

$$k_o^{ow}(s; s_{wr}^{ow}, s_{or}^{ow}), \quad k_o^{ow}(s; s_{wr}^{ow}, s_{or}^{ow}), \quad \text{for } s_{wr}^{ow} \leq s \leq 1 - s_{or}^{ow}.$$

Similarly, from (28) a corresponding capillary pressure function is obtained

$$P_c^{ow}(s; s_{wr}^{ow}, s_{or}^{ow}), \quad \text{for } s_{wr}^{ow} \leq s \leq 1 - s_{or}^{ow},$$

where the following values are used

$$(s_1^{ow}, pc_1^{ow}) = (0.2, -0.1), \quad (s_2^{ow}, pc_2^{ow}) = (0.8, -0.5). \quad (57)$$

Moreover, P^* is associated with the reference capillary pressure value \bar{P}_c introduced above

$$P^{*,ow} = \bar{P}_c. \quad (58)$$

We refer to Fig. 3 for a plot of these curves (red line).

Water-wet conditions. The following set of values for *water-wet* conditions is used:

$$k^{*,ww} = 0.4, \quad k_o^{*,ww} = 0.9, \quad s_{wr}^{ww} = 0.15, \quad s_{or}^{ww} = 0.25, \quad Nk^{ww} = 3, \quad Nk_o^{ww} = 2. \quad (59)$$

These choices give corresponding relative permeability curves

$$k^{ww}(s; s_{wr}^{ww}, s_{or}^{ww}), \quad k_o^{ww}(s; s_{wr}^{ww}, s_{or}^{ww}), \quad \text{for } s_{wr}^{ww} \leq s \leq 1 - s_{or}^{ww},$$

and via (28) a corresponding capillary pressure function

$$P_c^{ww}(s; s_{wr}^{ww}, s_{or}^{ww}), \quad \text{for } s_{wr}^{ww} \leq s \leq 1 - s_{or}^{ww},$$

with

$$(s_1^{ww}, pc_1^{ww}) = (0.2, 0.4), \quad (s_2^{ww}, pc_2^{ww}) = (0.7, -0.3). \quad (60)$$

Again

$$P^{*,ww} = \bar{P}_c. \quad (61)$$

We refer to Fig. 3 for a plot of these curves (blue line).